



# Mining CRRES IDM Pulse Data and CRRES Environmental Data to Improve Spacecraft Charging/Discharging Models and Guidelines

*A.R. Frederickson*

*California Institute of Technology, Pasadena, California*

*D.H. Brautigam*

*USAF Research Laboratories, Hanscom Air Force Base, Massachusetts*



Prepared for Marshall Space Flight Center  
under H-Order 34774D  
and sponsored by  
The Space Environments and Effects Program  
managed at the Marshall Space Flight Center

## The NASA STI Program Office...in Profile

Since its founding, NASA has been dedicated to the advancement of aeronautics and space science. The NASA Scientific and Technical Information (STI) Program Office plays a key part in helping NASA maintain this important role.

The NASA STI Program Office is operated by Langley Research Center, the lead center for NASA's scientific and technical information. The NASA STI Program Office provides access to the NASA STI Database, the largest collection of aeronautical and space science STI in the world. The Program Office is also NASA's institutional mechanism for disseminating the results of its research and development activities. These results are published by NASA in the NASA STI Report Series, which includes the following report types:

- **TECHNICAL PUBLICATION.** Reports of completed research or a major significant phase of research that present the results of NASA programs and include extensive data or theoretical analysis. Includes compilations of significant scientific and technical data and information deemed to be of continuing reference value. NASA's counterpart of peer-reviewed formal professional papers but has less stringent limitations on manuscript length and extent of graphic presentations.
- **TECHNICAL MEMORANDUM.** Scientific and technical findings that are preliminary or of specialized interest, e.g., quick release reports, working papers, and bibliographies that contain minimal annotation. Does not contain extensive analysis.
- **CONTRACTOR REPORT.** Scientific and technical findings by NASA-sponsored contractors and grantees.

- **CONFERENCE PUBLICATION.** Collected papers from scientific and technical conferences, symposia, seminars, or other meetings sponsored or cosponsored by NASA.
- **SPECIAL PUBLICATION.** Scientific, technical, or historical information from NASA programs, projects, and mission, often concerned with subjects having substantial public interest.
- **TECHNICAL TRANSLATION.** English-language translations of foreign scientific and technical material pertinent to NASA's mission.

Specialized services that complement the STI Program Office's diverse offerings include creating custom thesauri, building customized databases, organizing and publishing research results...even providing videos.

For more information about the NASA STI Program Office, see the following:

- Access the NASA STI Program Home Page at <http://www.sti.nasa.gov>
- E-mail your question via the Internet to [help@sti.nasa.gov](mailto:help@sti.nasa.gov)
- Fax your question to the NASA Access Help Desk at (301) 621-0134
- Telephone the NASA Access Help Desk at (301) 621-0390
- Write to:  
NASA Access Help Desk  
NASA Center for AeroSpace Information  
7121 Standard Drive  
Hanover, MD 21076-1320  
(301)621-0390



# Mining CRRES IDM Pulse Data and CRRES Environmental Data to Improve Spacecraft Charging/Discharging Models and Guidelines

*A.R. Frederickson*

*California Institute of Technology, Pasadena, California*

*D.H. Brautigam*

*USAF Research Laboratories, Hanscom Air Force Base, Massachusetts*

Prepared for Marshall Space Flight Center  
under H-Order 34774D  
and sponsored by  
The Space Environments and Effects Program  
managed at the Marshall Space Flight Center

National Aeronautics and  
Space Administration

Marshall Space Flight Center • MSFC, Alabama 35812

## Acknowledgments

This effort was accomplished with resources provided by NASA's Living With a Star (LWS) Space Environment Testbeds (SET) Program.



Available from:

NASA Center for AeroSpace Information  
7121 Standard Drive  
Hanover, MD 21076-1320  
(301) 621-0390

National Technical Information Service  
5285 Port Royal Road  
Springfield, VA 22161  
(703) 487-4650

***Mining CRRES IDM Pulse Data and CRRES  
Environmental Data to Improve Spacecraft  
Charging/Discharging Models and Guidelines***

---

**TABLE OF CONTENTS**

1.	Project Summary	1
	1.1 Introduction	1
	1.2 Objectives	2
2.	Details of Work Performed	3
	2.1 The Environment of High-Energy Electrons and Correlation to Pulsing	3
	2.2 Theoretical Determination of Electric Fields in the Samples	11
	2.3 Theoretical Determination of Conductivity in FR4 in Space	35
3.	Conclusions	39
4.	References	40
5.	Acknowledgements	40
6.	Appendix	41

# 1. Project Summary

## 1.1 Introduction

New information now allows for dramatic improvement in spacecraft charging guidelines and models, and improved comparison between ground test and in-space data. An intense study of discharges during the last three years has provided a new set of scaling laws for discharge pulses produced by electron irradiation of insulators.[1] Practical scaling laws predict the amplitude, duration and charge of discharge pulses as functions of insulator material, its size, and the radiation flux/energy spectra. It appears that a primary scaling law related to electric field is fundamental to all of the scaling laws. First and foremost, electric field internal to the insulator is the primary cause of discharges, their amplitude, and their rate of occurrence. [2] A number of subsidiary scaling laws are the result of the fundamental scaling law, and are also described in [2]. These new scaling laws were provided by recent data from ground testing, not from space.

However, scaling law space-data appears to be available from the internal discharge monitor (IDM) on the CRRES spacecraft. About ten years ago, when data from the IDM internal discharge monitor experiment was evaluated, these new scaling laws were not known. As a result, the IDM pulsing was tabulated against high-energy electron flux only, and not against any other parameter. [3] But, the raw data also contains pulse amplitude information not yet incorporated in the literature.

Because electric fields generated in insulators depend on the electron flux/energy spectra, pulsing is expected to correlate with spectra. The CRRES spacecraft and its IDM experiment experienced a variety of high-energy electron spectra. Mostly, they experienced electron flux in the heart of the electron radiation belts and also at geosynchronous altitude. These regions provide a large variety of electron flux/spectra.

In theory, one might be able to distinguish the occurrence of pulsing by thick insulators from the occurrence of pulsing by thin insulators on a spacecraft by correlating the history of pulses with spectral hardness. In ground testing, the pulse rate is seen to increase with increasing electron energy up to a maximum rate, and then decrease to nearly zero at much higher electron energy. This might assist in the resolution of anomaly studies, or it might allow one to pinpoint the source of electrostatic discharge problems on the spacecraft. For example, one might already know that pulses are occurring on a cable-run on the spacecraft, and that it only occurs when the spectra are hard. Ground testing proved that hard spectra generate pulsing in connectors but not in cables themselves. Thus the manufacturer would now know to simply change or redesign the connector leaving the rest of the cable harness alone. The thickness effect and other relations between sample pulsing and spectra can be investigated within the existing CRRES/IDM data set.

## 1.2 Objectives

**The Task is divisible into three studies:**

1. The first study mines new data from the CRRES flight and correlates Internal Charging and Discharging with the high-energy electron flux/energy spectra. This study is composed of three efforts:

a) Categorize the flux of electrons bombarding the IDM samples for both spectral hardness and the flux intensity as a function of time throughout the mission.

b) Tabulate the IDM data as a function of time for pulse event rate and pulse amplitude for each thickness of FR4 circuit board samples.

c) Correlate the pulse amplitude and event rate for each thickness with the spectral hardness and flux of the electron bombardment. This will provide the only in-space correlation between pulse amplitude or pulse rate and the electron flux/spectrum in space, and thereby will immediately improve existing design guidelines. To date, only the pulse rate has been documented, and it has been correlated with only the flux intensity, not the spectral hardness. [3]

2. The second study consists of theoretical determinations of the electric fields in the IDM insulators during the CRRES mission. The tested and proven code, NUMIT [4, 5], will be used for estimating the electric fields in the IDM FR4 insulators. An empirically determined, but approximate, value for dark resistivity of the FR4 will be used here.[6] The dark resistivity has little to no effect on the determination of the relative importance of the various spectra, so an approximate value is adequate. While holding all of the components of resistivity constant, one hopes to find that the calculated electric fields were greatest when the actual radiation spectra produced the greatest in-space pulse rate and amplitude. If this is indeed correct, then we have obtained evidence that our theoretical calculation of electric field is at least useful, even if not highly accurate. We will also have the first in-space confirmation of the potential guideline that pulse rate and amplitude scale with electric field.

3. In the third study, we propose to use NUMIT for estimating a range of validity for the dark resistivity in the IDM FR4 insulator. Based upon existing ground test data, we have approximate knowledge of the pulse rate as a function of the electric field in FR4. The IDM results provide the pulse rate in space, and thus tell us approximately what the electric field in the FR4 insulators must have been in space. And, from the proposed studies listed above, we know the flux spectra incident upon IDM during its periods of pulsing. NUMIT [4, 5] may then be used to calculate the electric field in the IDM samples as a function of the sample dark resistivity. By adjusting the resistivity parameter in the code, one can enable the code to predict the electric field that occurred in space. In this way, one is able to derive a crude estimate of the resistivity of the material in space.

## 2. Details of Work Performed

The Fortran statements were developed and the materials parameters were punched in for the FR4 sample. The software was initiated in order to calculate the electric field strength as a function of time during the last six months of the CRRES mission. A half hour later, the results were obtained and were better than expected. No adjustments to the code or material parameters were necessary in order to “fit” the data beyond the minimal adjustment for dark conductivity that was already known to be required. The value for dark conductivity that we obtained is reasonable, and can be checked later using new methods developed over the last year.

### 2.1 The Environment of High-Energy Electrons and Correlation to Pulsing

#### The First Study:

*The first study mines new data from the CRRES flight and correlates Internal Charging and Discharging with the high-energy electron flux/energy spectra. This study is composed of three efforts.*

*a) Categorize the flux of electrons bombarding the IDM samples for both spectral hardness and the flux intensity as a function of time throughout the mission.*

*b) Tabulate the IDM data as a function of time for pulse event rate and pulse amplitude for each thickness of FR4 circuit board samples.*

*c) Correlate the pulse amplitude and event rate for each thickness with the spectral hardness and flux of the electron bombardment. This will provide the only in-space correlation between pulse amplitude or pulse rate and the electron flux/spectrum in space, and thereby will immediately improve existing design guidelines. To date, only the pulse rate has been documented, and it has been correlated with only the flux intensity, not the spectral hardness. [3]*

#### 2.1.A Categorize the flux of electrons bombarding the IDM samples

AFRL fit differential flux spectra to a single exponential function  $j(E) = A \exp(-E/E_0)$ , where  $E$  and  $E_0$  are in MeV, and  $A$  has units of  $(\text{cm}^2 \text{ s sr MeV})^{-1}$ . These fits incorporate the MEA channels corresponding to 0.153 to 1.09 MeV, and HEEF channels corresponding to 1.6 to 4.55 MeV. MEA [10] and HEEF [11] are two electron spectrometers on the CRRES Spacecraft [2].

This does a nice job fitting and was considered lucky to have achieved such a simple structure to the spectra fits. Figure 1 is a plot of such a spectra for orbit 602 at altitude  $L=3.11$ . The fit parameters are on the plot.

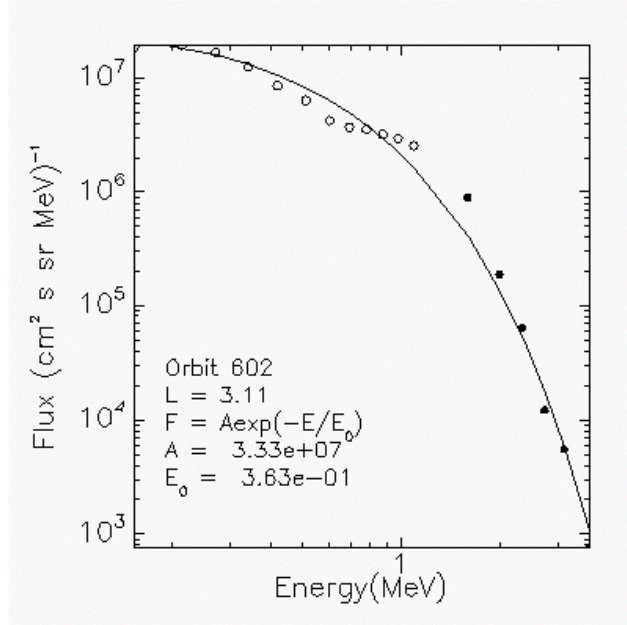


**Figure 1. A Fit to Spectra at a Brief Moment in Orbit 602.**

The fluence for each orbit leg, about 5-hours duration, for each channel, for  $L > 2.5$  (because of contamination issues) were determined as follows:

fluence / leg =  $60 * \sum_{n=1}^{N_{leg}} flux(E)$ , where flux(E) is the minute averaged flux (in above units) over

$75^\circ$ - $90^\circ$  pitch angle. The average over this range of pitch angle is taken in case there are low statistics and it is a good approximation for  $90^\circ$  for this range of pitch angle. The sum is over all minute intervals for  $L > 2.5$  to apogee. If there were more than 10 minutes missing per leg (which is critical if the data gap is around the location of peak fluxes), it was flagged, and adjacent legs were averaged later. The units of fluence are  $(\text{cm}^2 \text{ sr MeV})^{-1}$ . Figure 2 is a plot of the fluence spectrum for leg 1, the ascending leg, of orbit 602 compared to that of AE8max. Again, the fit parameters are on the plots.

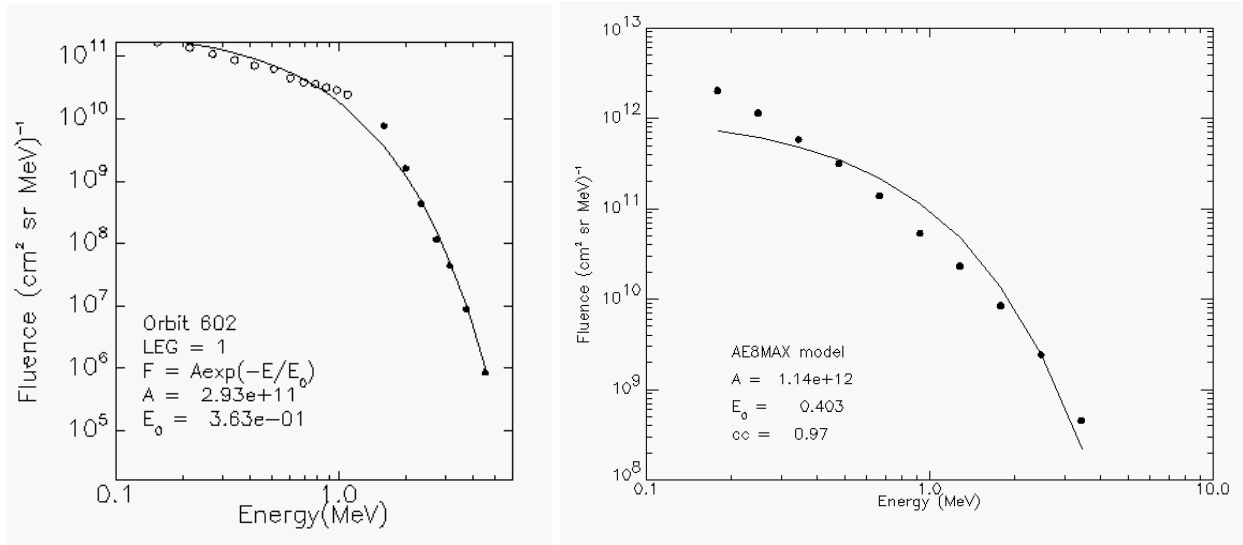


**Figure 2. Half-Orbit Fluence Spectrum for First Half of Orbit 602, and for AE8max in the Same Half-orbit.**

A plot of the parameters (log) A and  $E_0$  is given in Figure 3. This is a plot of Table 1 in the Appendix. This is a “processed” file where the legs without data were replaced with adjacent leg data, etc., and then adjusted with a weighted smoothing –  $x(i) = [x(i-1) + 2x(i) + x(i+1)]/4$ .

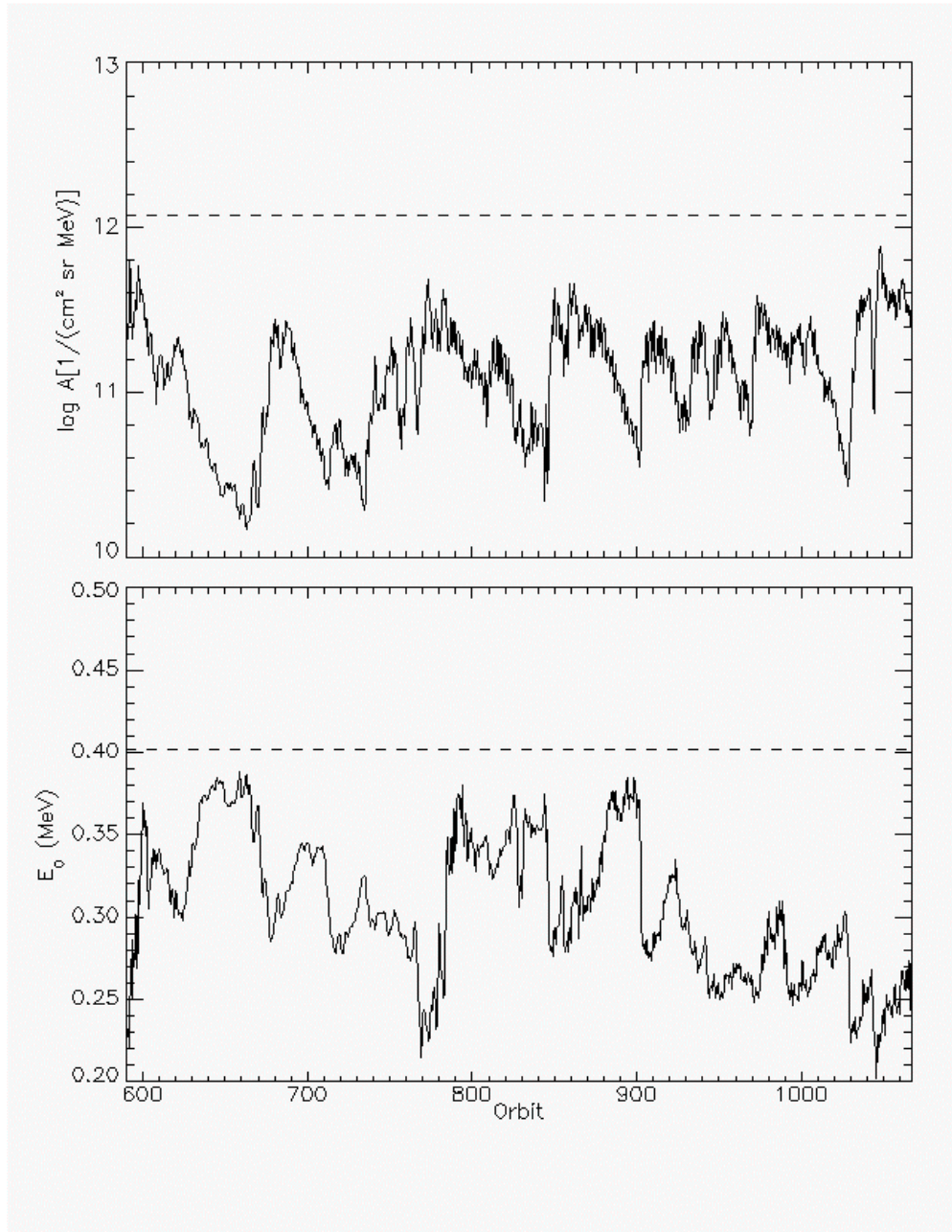


**Figure 3. History of Half-Orbit Spectral Fit Parameters Compared to Those of AE8max (dashed line).**

### 2.1.B Tabulate the IDM Data as a Function of Time

Although there is a table of pulses for the IDM Samples, it is much longer than the table of orbital spectra. It is best to simply display the pulse histograms from [1], in order to visually describe the pulse histories. Figure 4 shows both the pulsing history of all samples summed together, and the high-energy electron flux on the samples. Figure 5 describes the pulsing by each individual sample. See Reference 1 for full descriptions of the pulsing.

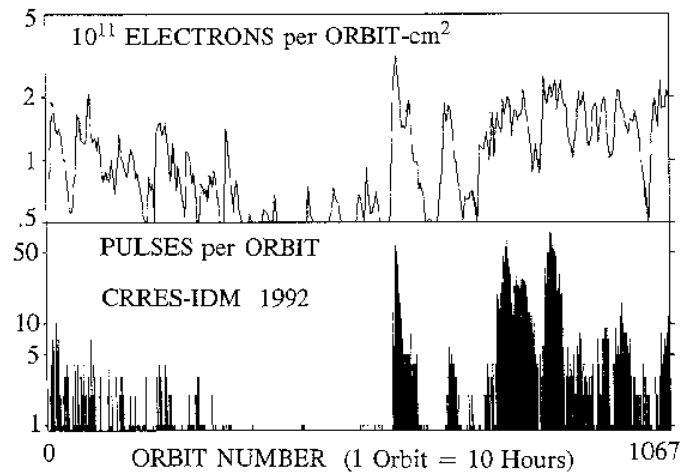


**Figure 4. High-energy Electron Flux incident on the Samples over the Life of CRRES, 1067 Orbits, and Pulse History Summed Over All CRRES/IDM Samples.**

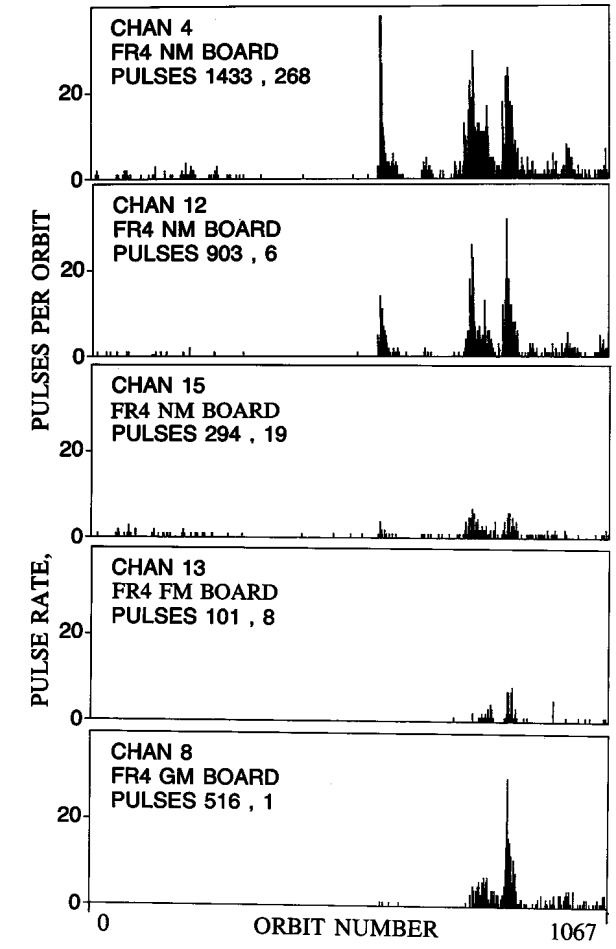


**Figure 5a. Pulse Rates for the FR4 Circuit Board Samples on CRRES/IDM.**

In this work, channel (sample) 8 is modeled because it has the well-defined electrostatic boundary condition of being grounded on both sides (See Figure 1). The other samples have a floating surface whose potentials were not monitored [1].

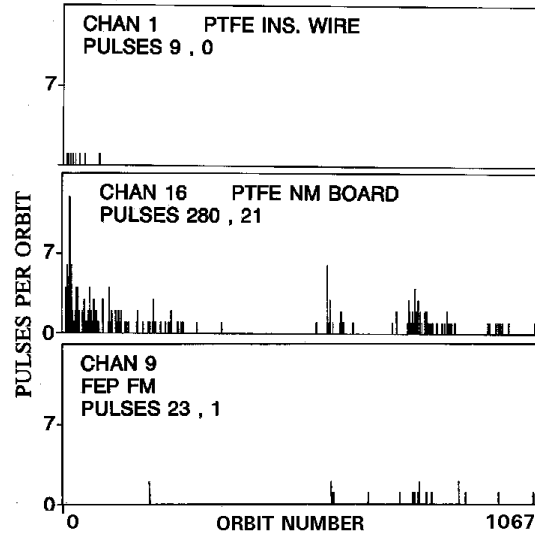


**Figure 5b. Pulse Rates on Teflon-based Samples on CRRES/IDM.**

Both the TFE wire and the TFE circuit board pulsed less frequently as fluence accumulated in space because this teflon becomes more conductive with increasing fluence [7]. Note that the FEP Teflon did not behave similarly. It does not become much more conductive with increased fluence.

The FR4 boards had the following thickness: Samples 4, 8, 12 and 13 were .317 cm thick. Sample 15 was .119 cm thick. Sample 13 had floating metal on its front surface making it difficult to analyze. Samples 4, 12 and 15 had free FR4 material at the front surface. Sample 8 had grounded copper on its front surface. All samples had grounded copper on the rear surface. Because sample 8 had the boundary of both surfaces grounded, while the other samples had unknown surface potentials, the analysis will concentrate on sample 8.

### **2.1.C. Correlate the IDM Pulse Data with Spectral Effects**

We learned that the pulsing correlates both with hardness and with flux intensity. The reasons for this correlation will be explained later in the section on calculating the electric field in Sample 8. It is informative to see the identical pattern of spectral effects for both electric field in the sample and correlation with pulse rate.

At the beginning of the project, it was hoped to correlate pulsing amplitude with spectral effects. As the spectral information was developed, it became clear that such correlation would not be very meaningful. We learned that the samples are integrating charge collection over at least five orbits in order to develop the highest electric fields. This is because the charge decay time constant substantially exceeds five orbits in the FR4 material. The spectral hardness does not hold for more than five orbits, usually only for two or three orbits. Although there are sufficient pulses to allow correlation of pulse rate alone with spectrum, there are too few large amplitude pulses to be so correlated.

Before considering the effects of electric fields, we look at simple correlations between spectral hardness and pulse rates by samples that frequently pulsed. This is not to imply that spectral hardness is a direct cause of pulsing. The occurrence of pulsing and the rate of pulsing are indicators of electric field strength. As a rough guideline, if the electric field rises above  $1 \times 10^7$  V/m, the pulse rate becomes noticeable, and then perhaps at  $3 \times 10^7$  V/m the rate exceeds 1/hour. The actual relation between pulse rate and field is not well known and these numbers are educated guesses [8]. Furthermore, the meaning of the correlation is further weakened because it was necessary to use data from the samples with floating front surface in order to have enough pulse data to perform the correlation.

We separated the  $E_0$  into two bins,  $(E_0)_1 < 0.3$  and  $(E_0)_2 > 0.3$  MeV. The logA are binned in increments of 0.2. Figure 6 shows the average pulse rates vs. logA. for each of the two energy ranges. For samples 4 and 12, the pulse rates are larger for the harder spectrum. These two samples are the same thickness as sample 8, of the same material, but have no copper electrode on the front (radiation incident) surface. Their front surfaces are floating. Since these two samples together produced about 2500 pulses they are the only ones with a sufficient number of pulses to allow meaningful graphs like Figure 6.

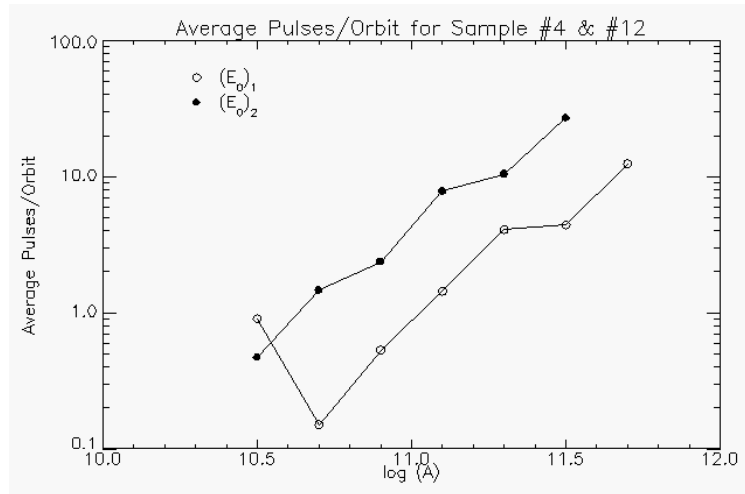


**Figure 6. Pulse rates by hard,  $(E_0)_2$ , and soft,  $(E_0)_1$ , spectra on samples 4 and 12 [1].**

The same type of analysis was done, but for 4  $E_0$  bins : 0.2-0.25, 0.25-0.3, 0.3-0.35, and 0.35-0.4 This results in Figure 7.

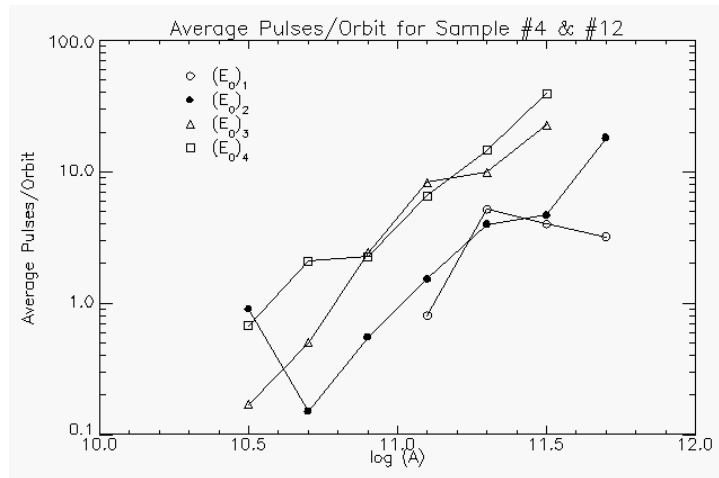


**Figure 7. Orbital Pulse Rates for Orbits Binned into Four Spectral “Hardness” Ranges.**

The reason for the effect of spectral hardness ( $E_0$ ) shown in Figures 6-7 should show up in the calculations of electric field in sample 8. Basically, both the soft and hard spectrum electrons stop in the first half of these samples. Therefore, much electron conduction occurs through the front surface as well as to the rear of the sample. But in the front surface region, the soft spectrum produces a larger dose rate per incident electron than does the hard spectrum, and thereby produces more radiation-induced-conductivity (RIC), as well as more secondary electron emission from the front surface than does the hard spectrum. This causes the soft spectrum to produce more charge leakage from the sample than does the hard spectrum. This will become clear in the section on electric field.

## 2.2 Theoretical Determination of Electric Fields in the Samples

### The Second Study:

*The second study consists of theoretical determinations of the electric fields in the IDM insulators during the CRRES mission. This topic was developed in the fourth quarter so it is described in detail. It required us to develop a new radiation transport capability that is not in the literature. We developed an algebraic algorithm for determining dose depth and charge current depth under isotropic electron radiation. Previous algebraic algorithms were only for normal incidence. Since this achievement might form the basis for a publication we describe it in detail.*

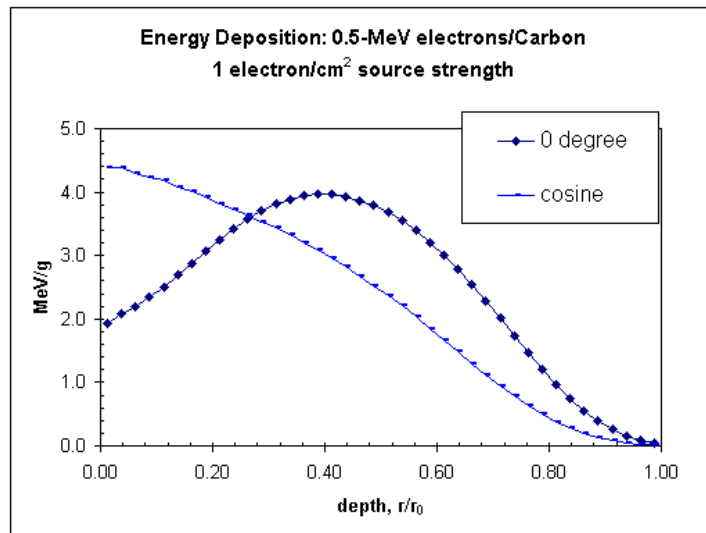
### 2.2.A Dose and High Energy Electron Currents in the IDM Insulator Samples

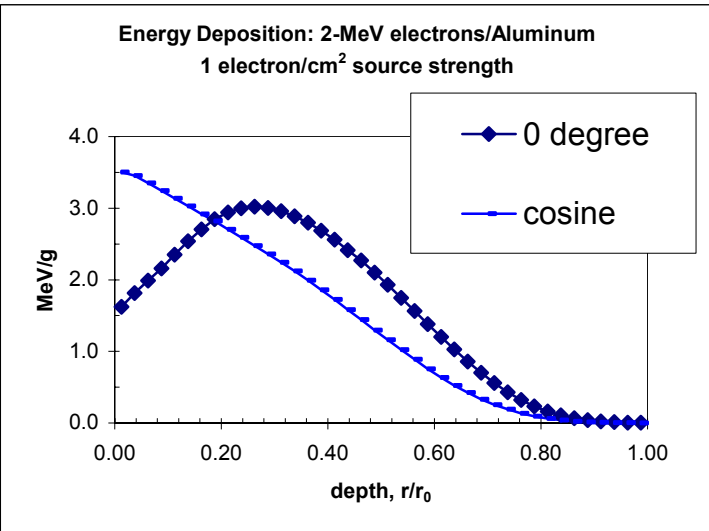
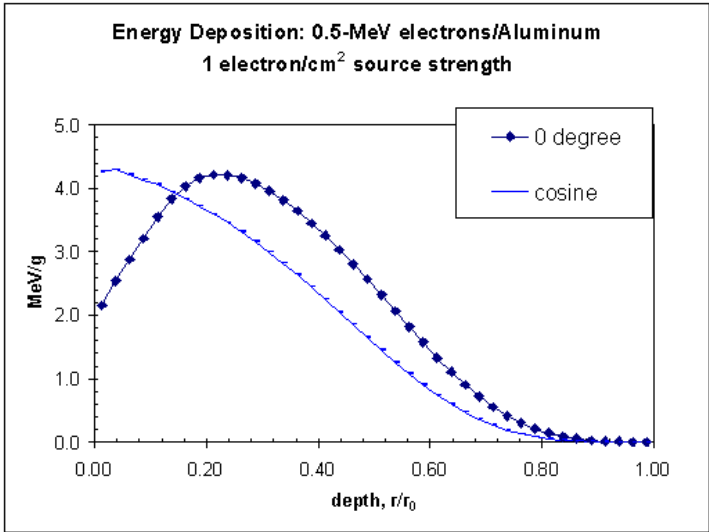
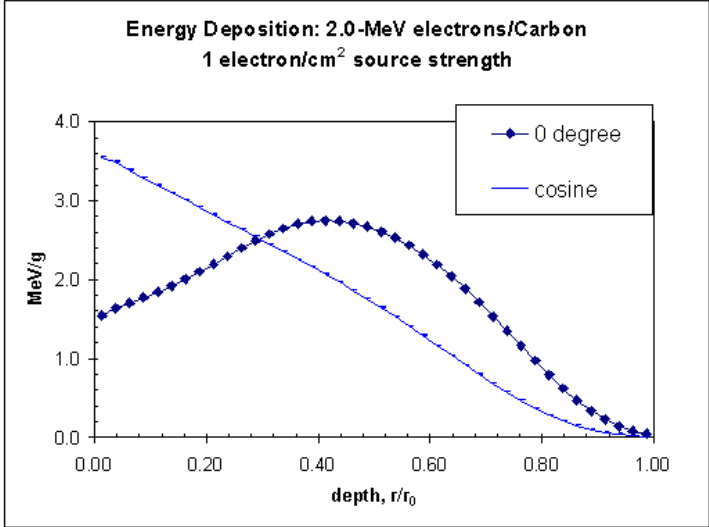
In order to calculate the charging of the insulators, we need to determine how the space radiation charge currents penetrate, and how the conduction in the material removes charge. Thus we need to determine the dose rate and the charge stopping in the material.

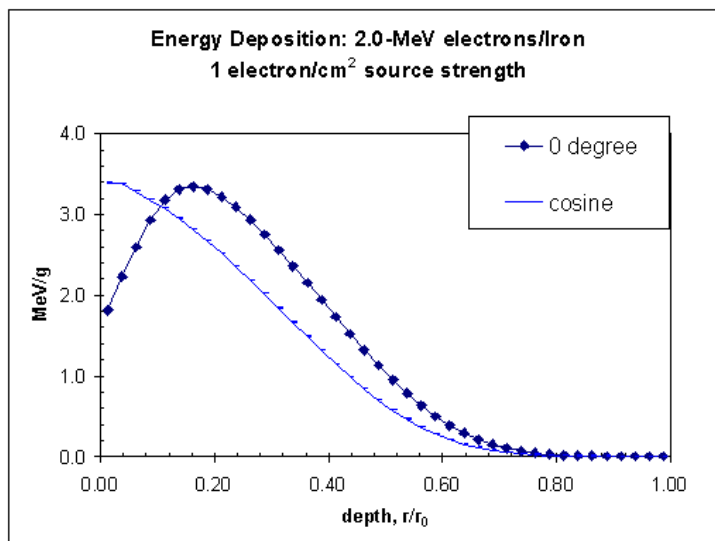
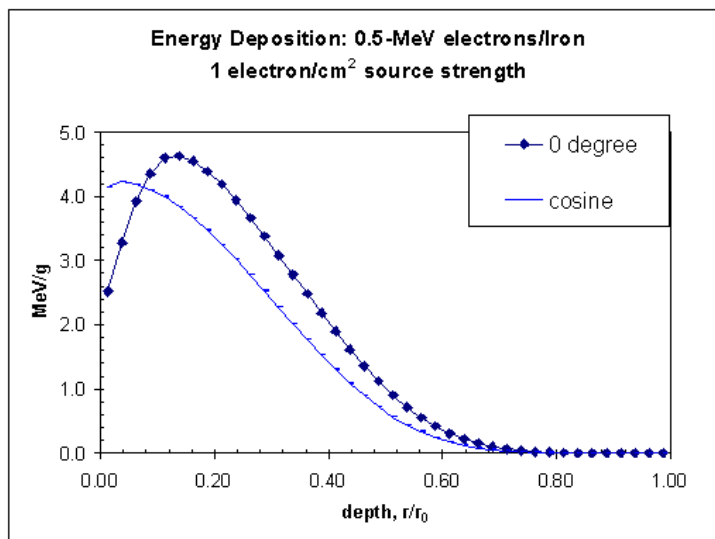
Each half-orbit will be characterized by an average spectrum. We determined this to be appropriate because the samples do not charge significantly during just one orbit. Thus, the average charge accumulation during the half-orbit will not be even fractionally bled off during its orbit, or, indeed, not for several more half orbits.

With the average spectrum defined, one could run a Monte-Carlo radiation transport code to determine the dose and high-energy electron charge currents in each half orbit. That would create a lot of expensive Monte-Carlo runs. Instead, we chose to use existing analytic charge transport codes that reproduce the Monte-Carlo data in normal incidence. We show how to alter the analytic code to produce the proper dose and current profiles for isotropic incidence. We determine a ratio, as a function of depth, between isotropic and normal incidence for both dose and current.

The ratio of dose by isotropic incidence to the dose by normal incidence can be determined from the following data. Note that in the radiation transport field, the term cosine implies isotropic flux. These data were provided by the MCNP code, although similar data would result from a number of codes.

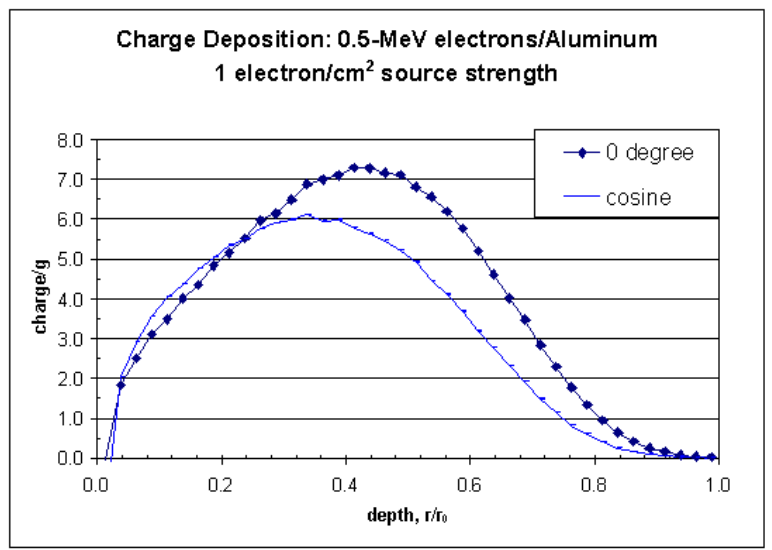
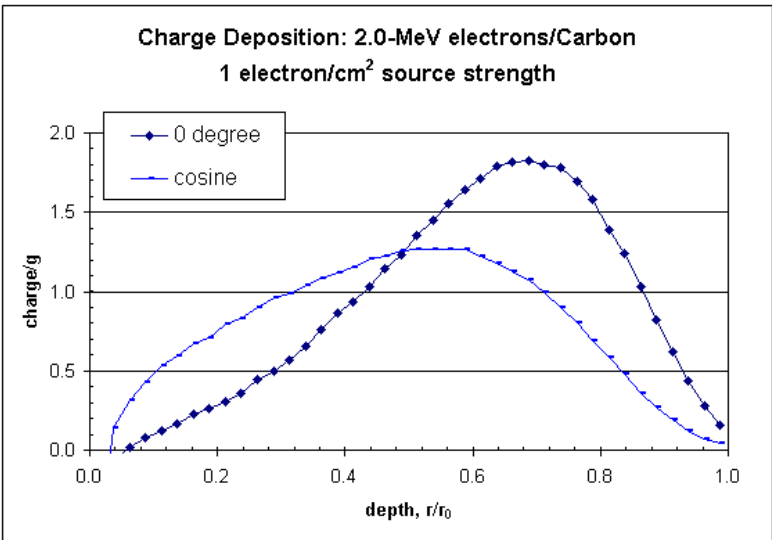
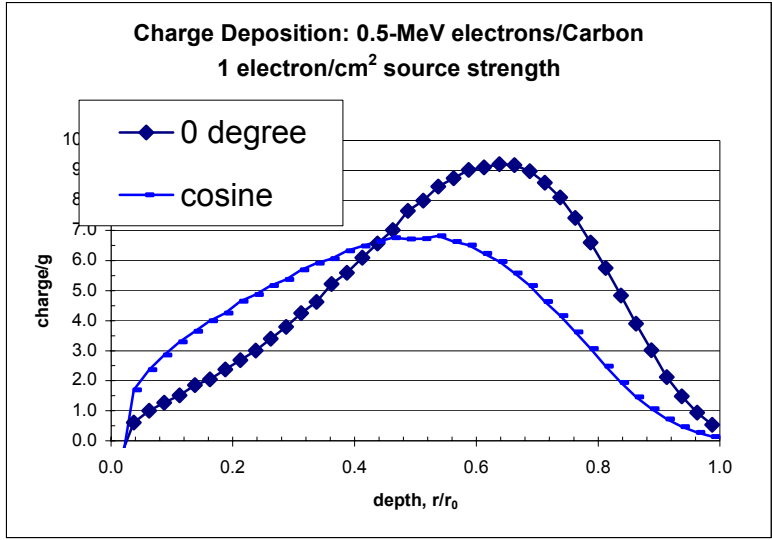


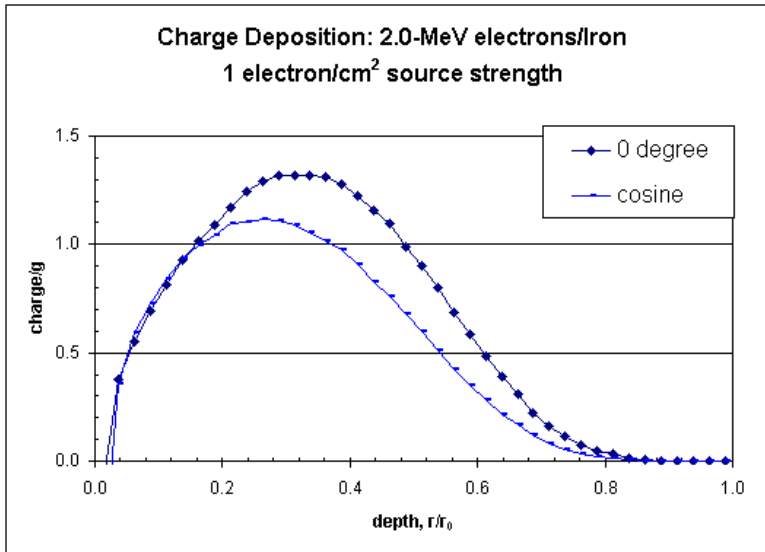
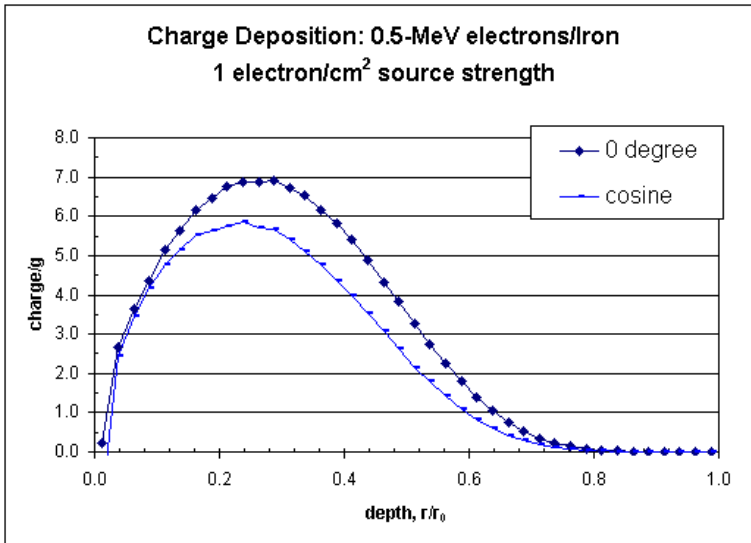
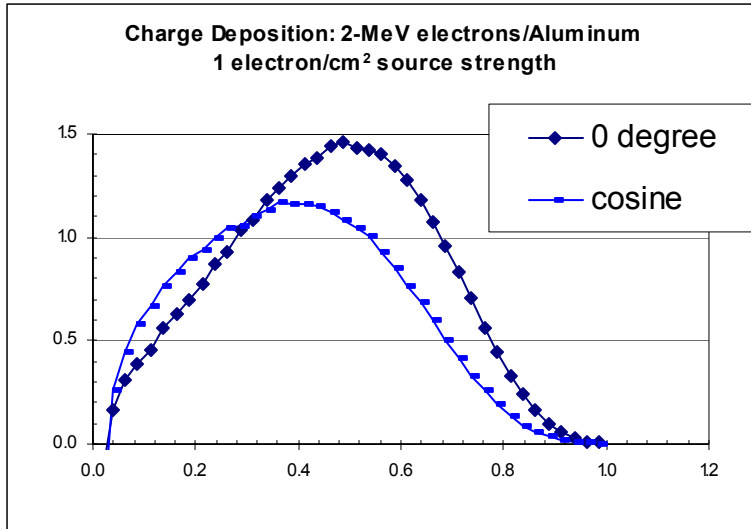




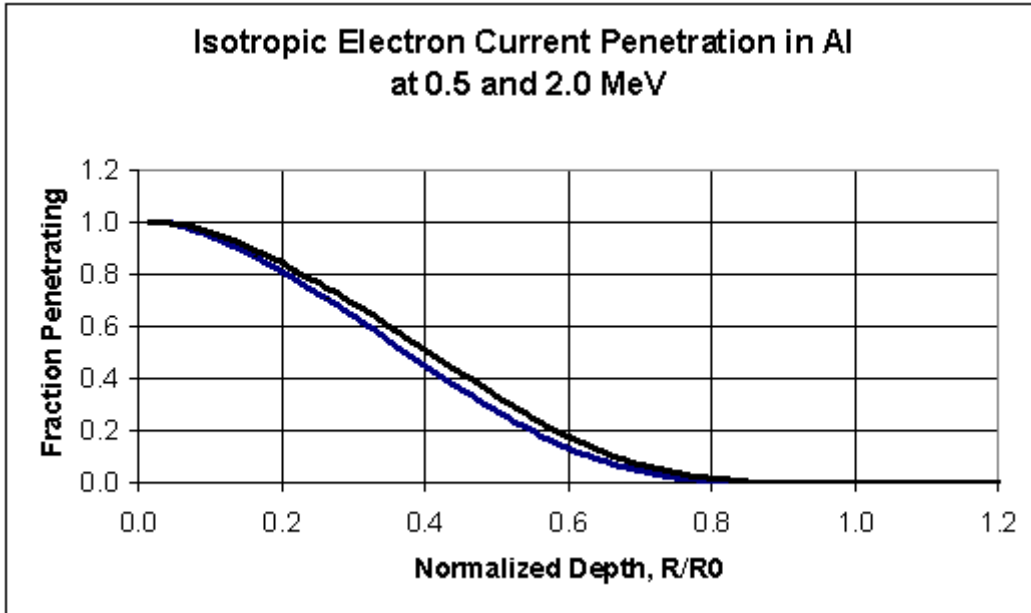
We will determine the ratio of cosine/normal for both dose and current. The ratios for Aluminum at 0.5 MeV and 2.0 MeV will be averaged at each relative depth,  $R/R_0$ . The ratio will then be fit to a function of normalized depth,  $R/R_0$ , called the Ratio Function. We will assume this to be the true ratio for our IDM samples at all energies.

The ratio of isotropic current to normal current is also needed.

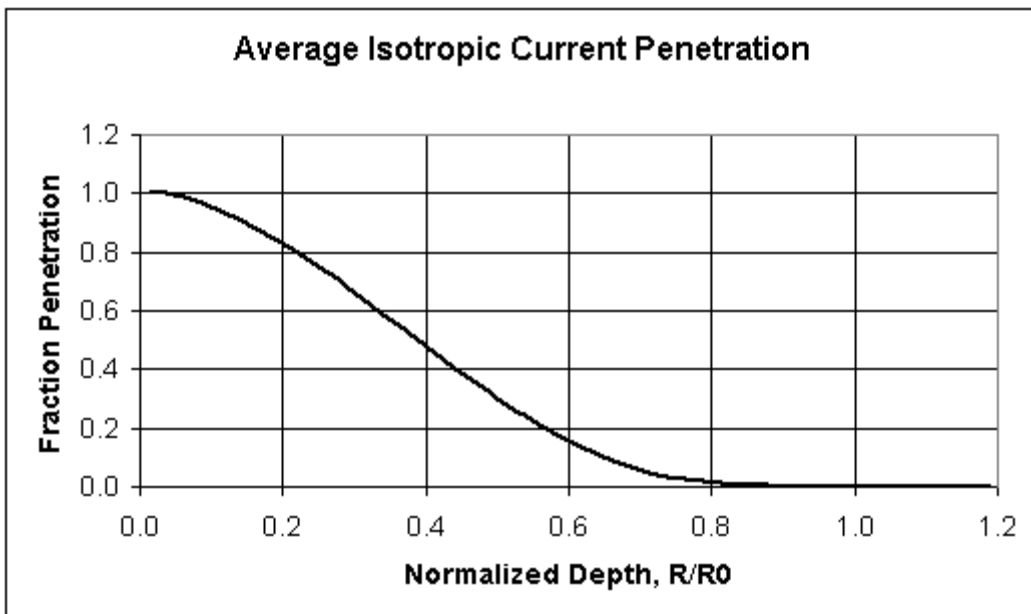




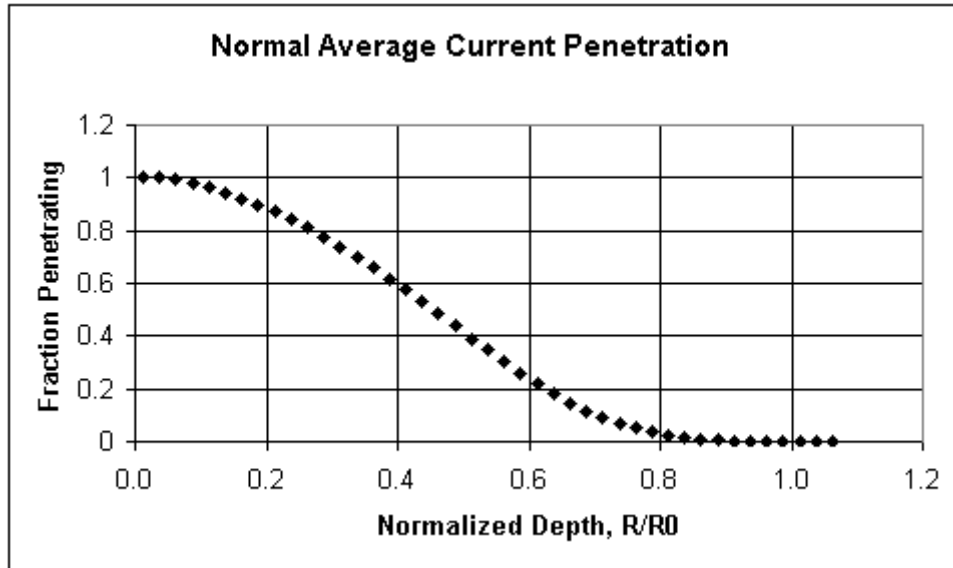
The next three graphs show the penetration of 2 MeV together with 0.5 MeV electrons determined by averaging over the two energies in Aluminum. This becomes our assumed penetration profile for all electrons in the range of interest in IDM, roughly 0.2 to 3 MeV. The first graph shows penetration of both 2 MeV and 0.5 MeV isotropic electrons.



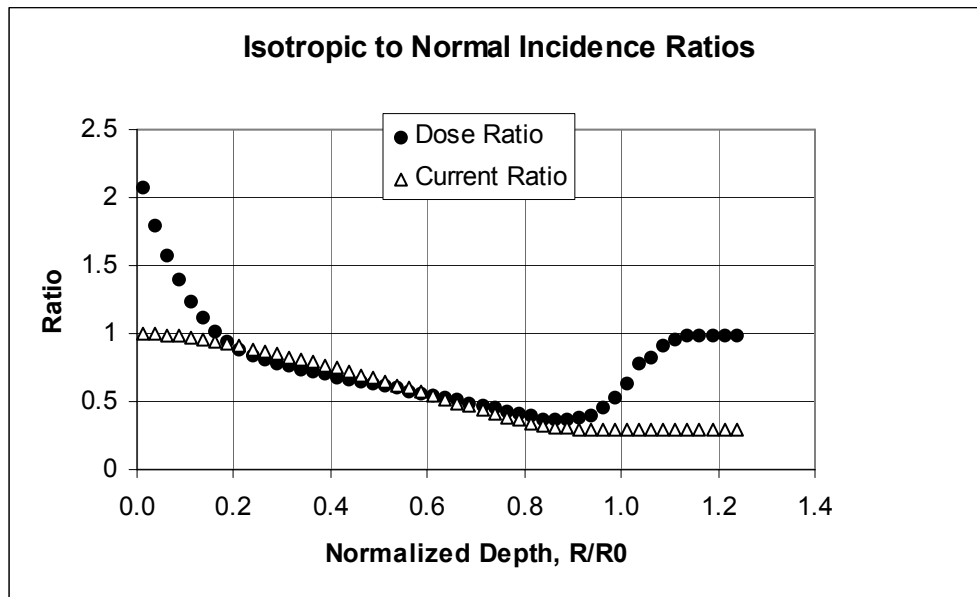
Since the penetration at both energies are similar, we will lump them together into one average isotropic penetration function shown in the following graph.



Similar analysis obtains the average penetration function for normal incidence shown in the following graph.



The dose ratio and the current ratio are both plotted in the following graph.



The dose and current ratios are fit to analytic functions so that they may be incorporated into the computer program, NUMIT, for calculation of electric fields in the IDM insulator samples. Application in the NUMIT code requires care that the fit-functions are not pathologic. A pathologic function is one that is used by the software in a range of the independent variable where wild fits are obtained. Our functions must provide reasonable fits over the depth range

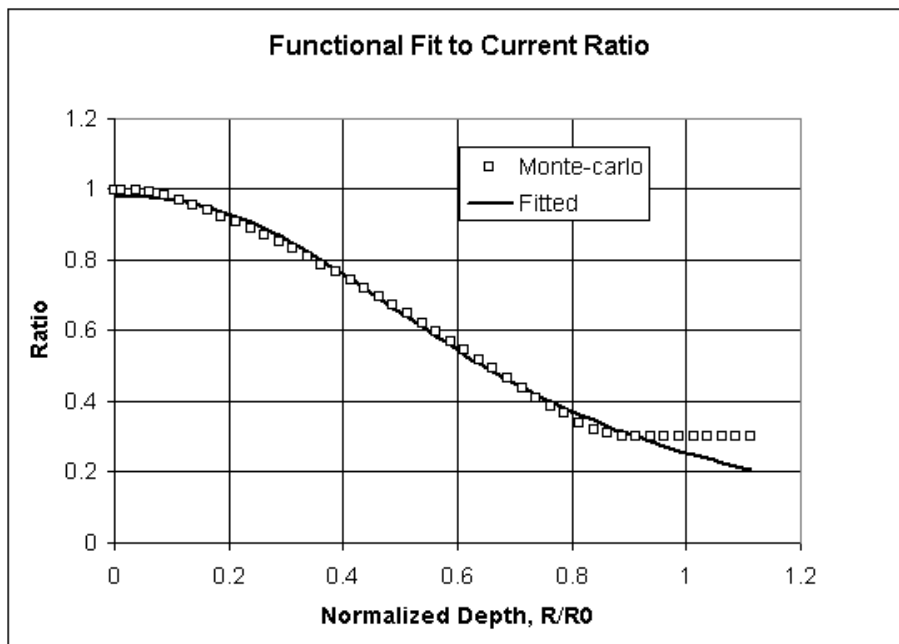
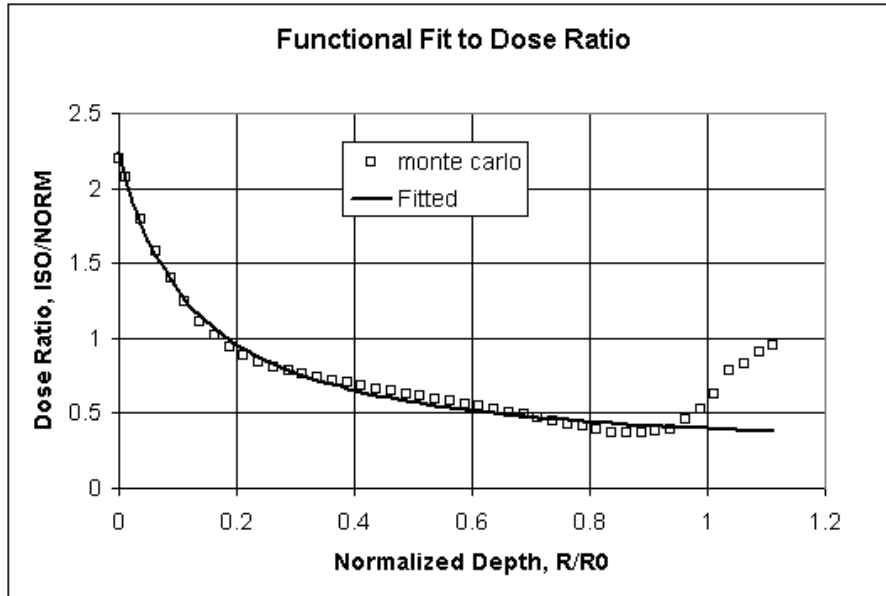
from 0 to  $R_0$ , the extrapolated range. Beyond  $R_0$ , the functions should simply remain in the range between 0 and 2 so that they do not return an unreasonable dose-depth or current-depth beyond  $R_0$ .

The functional fits are given by (x is 1.0 at  $R_0$ ):

$$doseratio = 1/(a + be^{-x})$$

$$currentratio = 1/(c + dx^{2.5})$$

where  $a = 3.7319028$ ,  $b = -3.2851211$ ,  $c = 1.0211457$ ,  $d = 2.905209$ .



The previous penetration current profiles are normalized to unity current just at, and beneath, the surface of the materials. In reality, the incident electrons are partially backscattered and therefore contribute neither actual current nor charge deposition. The backscatter must be properly entered into the NUMIT coding. If B is the backscatter fraction, then 1-B is the current actually penetrating.

In NUMIT, there is an expression for B under normal incidence that is called BAK. The normally incident current is corrected by the factor called (1-BAK) in NUMIT. The same feature is provided in the isotropic case by developing a backscatter fraction for isotropic incidence. We choose to use the factor (1-BAK\*\*0.5) which was developed by inspection of backscatter data in the literature in the range from 200 keV to 1.4 MeV. The function is reasonable (for our purposes) for atomic numbers less than about 40 (which covers nearly all insulators of interest).

There is another function, TRANS, that needs to be incorporated into NUMIT. It accounts for the attenuation of high-energy electron flux by the 0.2 mm aluminum cover plate and its structure. This function was previously published in Figure 5 of [3]. We fit this data to the following function for all energies above 0.29 Mev:

$$TRANS = \exp [a + b/(MeV)^2] ,$$

where a = 1.4754217 and b = -0.11595791.

TRANS is near-zero (or negative) below 0.29 MeV, rises to 1 (steradian) at 0.3 MeV, 3 (steradians) at 0.6 MeV and 4 sr from 1 MeV and above. If there were no cover plate, the TRANS function would be simply  $2\pi$  steradians at all energies.

TRANS is used as follows. Section 4.1.A, provides the space radiation intensity spectra in the form  $I = A \cdot \exp(-T/T_0)$  where T is the energy in MeV, and A is the Flux coefficient in units of  $(cm^2 \cdot s \cdot sr \cdot MeV)^{-1}$ . Note that A does not directly tell one the current density to a flat plate. "A" describes the current density to the surface of a sphere. The current density normal to one side of the surface of a sphere, covering  $2\pi$  steradians, is  $2\pi I$ . The current density to a flat plate is  $1/4$  of the current density to the spherical surface because essentially all of the current is off-normal so that the integral over angle of incidence provides the  $1/4$  factor. Thus, considering the form of the space radiation flux expression, and the attenuation by the cover plate, the space radiation (Flux) current density normal to the planar surface of the sample is given by:

$$J_{inc}(T) = 1/4 * TRANS(T) * A \exp(-T/T_0) .$$

With this information, NUMIT calculates dose and current penetration into the insulator material. After calculating the dose and current flows as if they were due to normally incident high-energy electrons, these are multiplied by the dose and current ratio functions (described above) in order to change them into dose and current for isotropic electrons.

Normally, NUMIT performs its calculations for monoenergetic electrons incident normally on the sample. NUMIT must be modified to handle the case for isotropic electrons incident on

planar samples with a wide distribution of energies. We will divide the incident energy into nearly monoenergetic “bins”, each bin about 100 keV wide, and with effective energies at 0.2, 0.3, ....., 4.0 MeV. The spectrum is divided into monoenergetic energies. The algebraic modification for isotropic flux is described above. This algorithm is new to our knowledge, and would be a positive contribution to the professional literature if it were expanded to a wider energy range. For our purposes, it needs to be good only over an energy range from 0.2 to 2 MeV, and approximate from 2 to 4 MeV.

For purposes of radiation transport (fast electrons), we continue to require that the elements that comprise the sample to be modeled as one equivalent-atomic number. For example: 1) most polymers can be modeled as carbon, 2) silicon and aluminum can be considered to be nearly identical, and 3) a homogeneous mix of materials can be modeled by averaging their atomic numbers. These assumptions produce the greatest error when a high atomic number material of substantial thickness is adjacent to a low atomic number. In our case, the “1-ounce” (30 mg/cm<sup>2</sup>) copper electrode interface to the FR4 epoxy forms a transport issue that our algebraic methods do not fully model. It is estimated that the effect is of the order of ten percent in the dose and charge deposition in the FR4 right at the interface. The error falls to negligible ten mils beyond the interface in the FR4. The overall effect of this error on the peak electric field in the FR4 is presumed to be no more than ten percent. An accurate estimate is possible using detailed monte carlo radiation transport codes as source input to NUMIT, but it is not felt to be profitable at this time.

As indicated in earlier reports, we used the Berger (National Academy of Sciences Monograph 1133) particle stopping tables for CSDA to determine the appropriate electron energies. FR4 circuit board is 1.85 grams/cc density, so that:

- a) Sample 15 is .119 cm thick is 202 mg/cm<sup>2</sup> thick, or more than 500 keV CSDA electron thick.
- b) Samples 4, 12 are .317 cm or more than 1.1 MeV CSDA electron thick.
- c) Sample 8 has 30 mg/cm<sup>2</sup> copper (1 oz/sq-ft or 1.3 mils) on the front surface in addition to the aluminum, thus is more than 1.2 MeV CSDA electron thick.

Since the CSDA thickness of the samples is about 1 MeV electron, the space environment must be well characterized for electrons from 200 keV up to 2 MeV. Electrons below 200 keV cannot penetrate the 8-mil (55 mg/cm<sup>2</sup>) Aluminum cover of the IDM instrument. Our lowest energy bin is centered at 0.3 MeV. Additionally, the flux of all electrons above 2 MeV is needed to estimate the dose. This is the applicable range for environmental electron energy. The MEA and HEEF instrument data tabulated at AFRL are appropriate for this range.

Outline of the Logical Flow of the JOCALC Program.

1. First we choose a specific energy bin,  $T_k$ . At this energy, we calculate the dose-depth and current-depth profile under the assumption of normal incidence for a unit intensity.
2. Since we use exponential-law spectra, we must weight the energy bin accordingly. The transmission of externally isotropic flux through the aluminum cover plate as a function of

energy has been determined. We have fit this function over the energy range of interest, and call it TRANS(T). Jinc is multiplied by the product TRANS(T).

3. Next we determine a ratio (function) for the isotropic dose divided by the monoenergetic dose at every depth over the penetration range of the incident electron. The ratio is a function of depth. It is accomplished here for energy bin  $T_K$ . This can be done over a finite energy range from 0.3 to 4 MeV with just one function by normalizing the depth to units of extrapolated electron range as discussed above. In the literature, there is an additional algebraic function for range-energy that makes our approach possible. The initial dose-depth (which was for normal incidence) is now multiplied by the function ratio-depth.

4. A similar ratio function is determined for the normally-directed current of high-energy electrons penetrating the sample. Because of the sample symmetry, the radiation driven current flows in the normal direction through the sample.

In steps 3 and 4 we have generated relative dose-depth and current-depth curves for the energy  $T_K$  electrons.

5. The dose-depth and the current-depth produced by energy bin  $T_K$  is accumulated in the arrays. We now return to the top of the logic flow and proceed again with another energy bin.

6. When the dose and current produced by all of the energy bins from 0.3 to 4 MeV is accumulated, this number is multiplied by high energy electron current flux, JINC, and a units conversion factor for flux to dose in rads/second.

The physics must be consistent even though the language of flux often uses inconsistent vocabulary. Our samples are one dimensional, and we are concerned with the incident current in the normal direction. But, the fast electrons are distributed isotropically in space. (This, despite their pitch angle distribution, is a result of the spinning spacecraft and our willingness to approximate when it simplifies the process.) When developing the ratio function in steps 3 and 4 above, one must use the proper monte carlo modeling to determine the result of an externally isotropic flux. Since our samples are planar, the incident flux (particles/sec-cm<sup>2</sup>-SR-MeV) is given by the cosine of the angle of incidence. One must choose the Monte-Carlo transport code option "cosine distribution." That is why we determined the ratio functions for the cosine law flux Monte-Carlo data, above.

For a bromated epoxy such as FR4 printed circuit board: density=1.85, atomic number Z=19, atomic weight AW=38, dielectric permittivity EP = 4.5E-11 Farads.meter.

### **2.2.B Calculations of Electric Field in the IDM Insulator Samples for Nominal Conditions**

The electric fields are calculated by the Fortran program NUMIT. NUMIT is described in A. R. Frederickson, "Radiation Induced Electrical Current And Voltage In Dielectric Structures," AFCRL-TR-74-0582, 1974.

The Fortran statement functions for the several currents describe the dielectric physics in the problem:

GAO(J) = radiation current produced by the penetrating electrons at depth J.

GA1(J) = V0\*E(J)\*RO(J)\*\*DE, is the radiation-induced conductivity (RIC) current at depth J where E is electric field in V/m, RO is dose rate in rads/s, and DE is a constant typical of each material but usually lying between 0.5 and 1.0. V0 is typically called  $k_p$  in the literature. The coefficient of radiation induced conductivity, V0, has not been determined for the FR4 material in prior tests, so a typical value will be chosen from the literature [3] as a starting assumption. The coefficient of radiation-induced conductivity is assumed to be  $V0 = k_p = 3 \times 10^{-16}$  (s/ohm-m-rad).

GA2(J) = V1\*E(J)\*RO(J)\*T is the delayed radiation-induced conductivity current where T is time, and the product RO\*T indicates the accumulation of damage that produces such conductivity. Lengthy experiments are required to evaluate the parameter V1. However, total dose also generates damage that decreases the conductivity by the generation of traps. The trap generation must also be evaluated to determine the net quantitative balance between the two competing effects. Such work would require further research. In this research, we can only determine the initial direction of the net effect. It is clear from this study that the conductivity of FR4 decreases after exposure to space and/or radiation. Here, V1 is set to zero. Recent laboratory tests corroborate this result. [6] The net effect in space is that the conductivity of the FR4 sample decreases as the rest of this report indicates.

GA3(J) = V2\*E(J) is the dark conductivity current at depth J. V2 is typically called the dark conductivity in the materials literature using the symbol  $\sigma$ . Conductivity,  $\sigma$ , of the FR4 sample is herein initially estimated from the charge decay time constant recently measured on another FR4 sample recently manufactured, 15 years after manufacture of sample 8. The charged surface decayed by 1/e in about one day. From the formula,  $\tau = \epsilon/\sigma$ , with  $\epsilon = 4.5 \times 10^{-11}$  F/m, the conductivity,  $\sigma$ , is initially assumed to be  $5 \times 10^{-16}$  (ohm-m)<sup>-1</sup>. See Reference [5].

TIME FOR A HALF ORBIT = 18,000 Seconds.

The incident current density of high-energy electrons in space is briefly noted in two publications [1,2]. In the first publication, the “all” electron flux varies over two orders of magnitude, and when a typical value when pulsing occurs, the all electron flux is  $1 \times 10^{11}$  (cm<sup>2</sup>-orbit)<sup>-1</sup>, which corresponds to  $4.44 \times 10^{-9}$  (A/m<sup>2</sup>) (See Figure 4). In the second publication, the flux of all electrons above 0.85 MeV is provided, typically  $1 \times 10^{10}$  (cm<sup>2</sup>-orbit)<sup>-1</sup> when pulsing occurs. Approximately 90% of the high-energy electron flux occurs below 1 MeV.

Figure 4 shows the history of pulsing and electron flux at the CRRES spacecraft.  $1 \times 10^{11}$  electrons/cm<sup>2</sup> orbit is equivalent to  $4.44 \times 10^{-9}$  A/m<sup>2</sup>. Sample 8 is chosen for the calculations because it is the best-controlled sample. Both of its surfaces are held grounded. It is therefore appropriate to perform initial calculations of charge accumulation in the IDM/CRESS sample 8 with an incident high-energy electron flux of  $4 \times 10^{-9}$  A/m<sup>2</sup>. The thickness of the sample is 0.312 cm between copper electrodes each of .0025 cm thickness described in Figure 8.

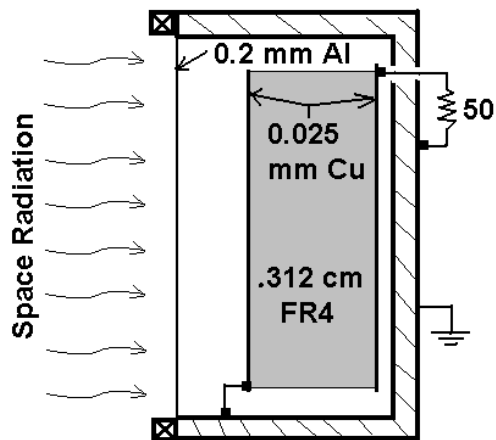


**Figure 8. Sample 8 in its mounting on the CRRES spacecraft.**

The 0.2 mm cover plate and the structural box walls prevent full incidence of isotropic flux. Instead of  $2\pi$  steradians, there is only 4 steradians incident. Both copper electrodes are grounded.

It is important to note that this thickness exceeds the range of a 1 MeV electron as shown in Figures 9-11. 90% of the electron flux in space is below 1 MeV.

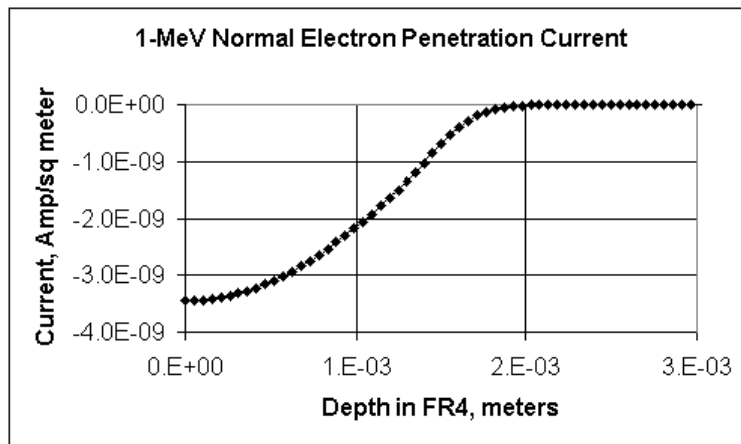


**Figure 9. Penetration and stopping of normally incident 1 MeV electrons,  $-4 \times 10^{-9}$  Amperes/m<sup>2</sup>, in the FR4 sample 8.**

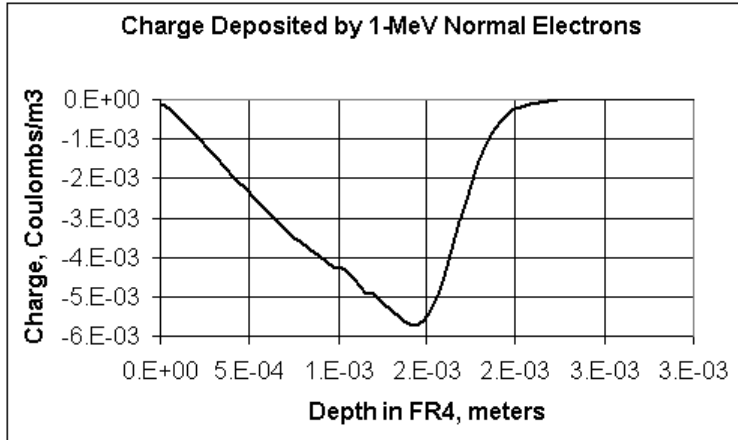


**Figure 10. Stopping of charge in sample 8 bombarded with 1 MeV normally incident electrons at a flux of  $-4 \times 10^{-9}$  Amperes/m<sup>2</sup>.**

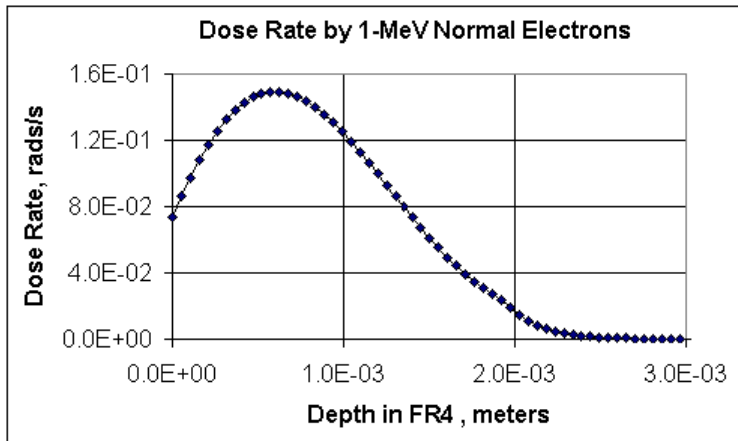


**Figure 11. Dose rate in sample 8 produced by 1 MeV normally incident electrons at a flux of  $4 \times 10^{-9}$  Amperes/m<sup>2</sup>.**

As charge is deposited at a rate shown in Figure 10, the electric field builds up. As the E-field builds, conduction currents grow to counter further build-up. The net result for 1 MeV normal electron irradiations described in Figures 9-11 produces an electric field shown in Figure 12.

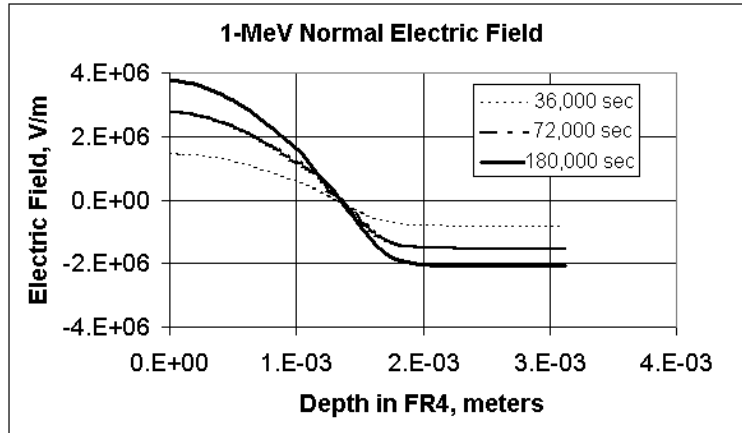


**Figure 12. Electric field at three times in sample 8 exposed to the radiation of Figures 9-11.**

At about 180,000 seconds, the conduction currents had grown to fully counter the deposition of the high-energy electrons. The total current, primary electrons plus conduction electron (and holes) then become constant everywhere in the sample. The current stabilized at about  $-1.3 \times 10^{-9}$  A/m<sup>2</sup> throughout the sample while the electric field remained steady with the profile shown in Figure 12 at 180,000 seconds. The sample attained steady state.

Since electrons are nearly isotropic in space, it is better to discuss the isotropic case. Figures 13-16. depict the case where the mono-energetic electrons arrive in isotropic distribution with an incident current density at  $-4 \times 10^{-9}$  A/cm<sup>2</sup>, similar to the normally directed current density. The isotropic 1 MeV electron current attenuates more quickly in the sample as shown in Figure 13 and deposits charge (Figure 14) generally less deep than does 1 MeV electron current in normal incidence. The dose also attenuates more rapidly.

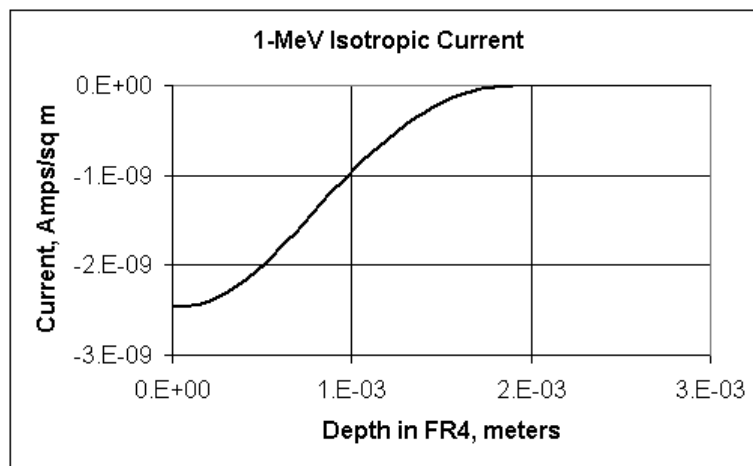


**Figure 13. Attenuation of 1 MeV isotropic incident electron current on sample 8.**

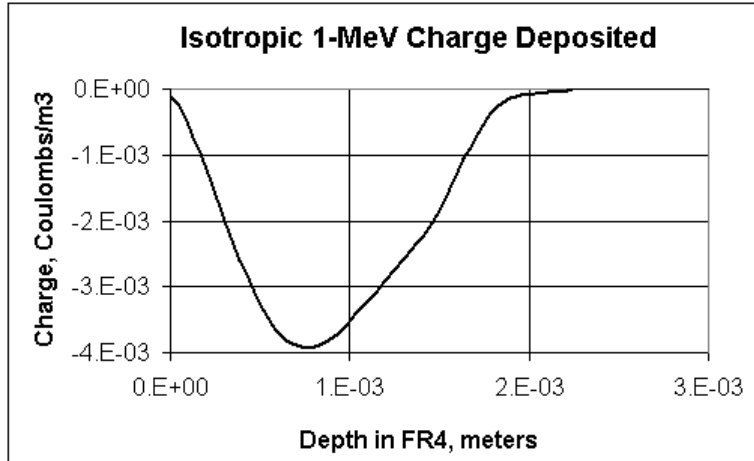


**Figure 14. Deposition of 1 MeV isotropic electrons in sample 8.**

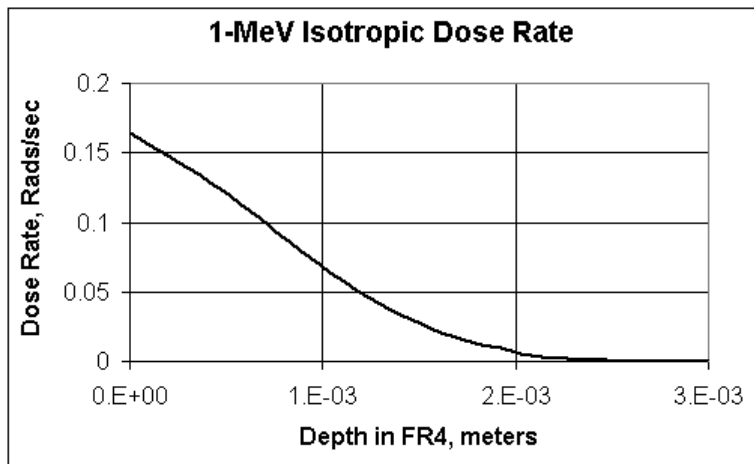


**Figure 15. Dose rate produced by isotropic 1 MeV electrons at  $-4 \times 10^{-9}$  A/m<sup>2</sup> Flux.**

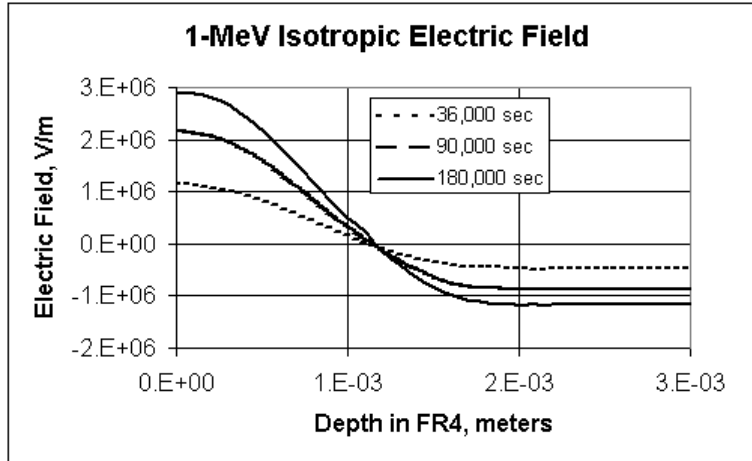


**Figure 16. Electric field developed in sample 8 under 1 MeV isotropic electrons at  $-4 \times 10^{-9}$  A/m<sup>2</sup> Flux.**

The net results of altering the 1 MeV electron flux from normal to isotropic incidence is to decrease the steady state electric field strength and to place the depth of the zero-field plane shallower as shown in Figure 16. Primarily, the isotropic electrons provide nearly twice the dose rate in the front of the sample and thereby develop more conductivity to remove the electrons to the front after they are deposited. Compared to normal incidence, more of the removal of stopped high-energy electrons proceeds to the front electrode, and the steady state constant current through the whole sample to the rear is about  $0.7 \times 10^{-9}$  A/cm<sup>2</sup> (about  $-1.3 \times 10^{-9}$  A/m<sup>2</sup> in normal incidence).

In preparation for using the actual data from space, we next survey the effect of varying the resistivity of the sample. Why? Under the typical conditions for our sample, it does not develop enough electric field in space fluxes to generate pulsing. More than  $1 \times 10^7$  V/m is needed to induce occasional pulsing (one per day), and  $1 \times 10^8$  V/m is needed to generate pulses faster than, 10 per hour [8]. The prior figures indicate that we may not achieve sufficient electric field in the typical FR4 sample to generate pulses. Where did we get typical FR4 parameter values?

The radiation-induced conductivity in FR4 has not been measured to our knowledge. But most highly-insulating polymers are in a not-too-wide range[3]. If R is the dose rate (rads/s), then conductivity is given by  $\sigma = k_p R^\Delta$ . The coefficient,  $k_p$  is here assumed to be  $3 \times 10^{-16}$  (s/ohm-m-rad) from [3]. The exponent,  $\Delta$ , usually lies between 0.5 and 1.0, typically close to 1.0 at our dose rates. These values are used in our work here as “typical” values, and were used to develop Figures 9-16.

The dark conductivity current is given by a conductivity coefficient,  $\sigma$ , times the electric field. Conductivity,  $\sigma$ , of the FR4 sample is herein initially estimated from the charge decay time constant recently measured on another FR4 sample recently manufactured, 15 years after manufacture of sample 8. Figure 12 in [5] shows that the FR4 charged-surface decayed by 1/e in about one day. From the formula,  $\tau = \epsilon/\sigma$ , with  $\epsilon = 4.5 \times 10^{-11}$  F/m, the conductivity,  $\sigma$ , is therefore initially assumed to be  $5 \times 10^{-16}$  (ohm-m)<sup>-1</sup>. This conductivity is called the “typical”

conductivity of our sample, and was used to develop the data in Figures 9-16. The decay time-constant method is described in [4]. Handbook values for conductivity in insulators are suspect for reasons described in [4,5], and are generally much larger than this, our typical value.

The pulsing by a sample is an indicator of the electric field strength in the sample. Pulsing by sample 8 during the CRRES mission is shown in Figure 17. Inspection of Figure 4 indicates that the high-energy electron flux was as high early in the mission as it was late in the mission, yet the sample did not pulse early. It is believed that the conductivity changed due to radiation in space. Recent ground testing also indicates that FR4 material needs to be exposed to radiation before it easily produces pulsing. [6]

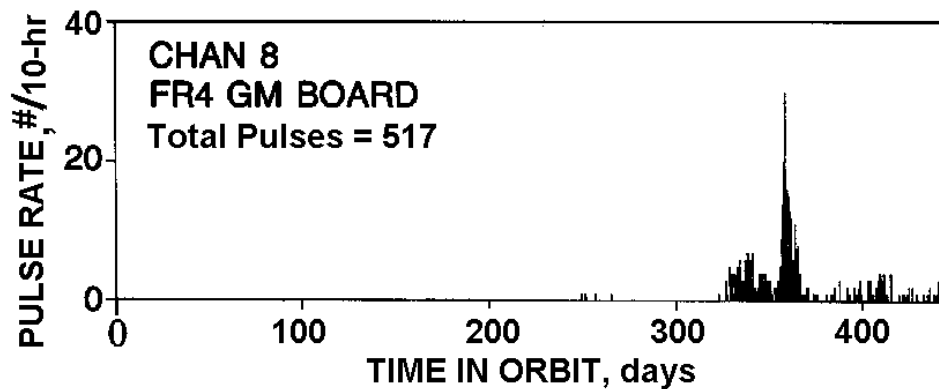
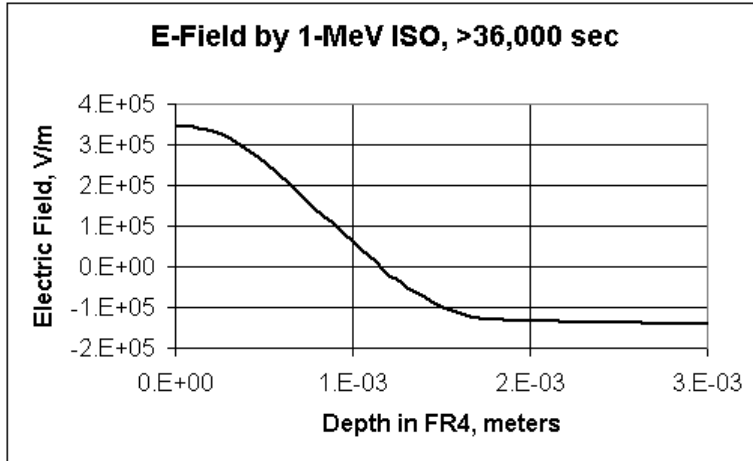


Figure 17. Pulse History for CRRES/IDM Sample 8. Pulsing begins after 245 days in space. [1]

### Effects of Varying The Conductivity

Next, we take a brief look at the effect of varying the conductivity of the FR4 sample. First we raise the dark conductivity by a factor ten. The calculation uses 1 MeV isotropic electrons at  $4 \times 10^{-9} \text{ A/cm}^2$ , as in Figure 16. Figure 18 provides the result that the steady state electric field is decreased almost a factor ten relative to Figure 16, and this occurs much earlier. Of course, lowering the resistivity causes the time constant to be smaller, and therefore steady state is achieved earlier.



**Figure 18.** In this test, the bulk conductivity was raised a factor of ten over the “typical” FR4 value. It resulted in nearly a factor of 0.1 reduced electric field compared to that (Figure 16) of the typical FR4. Steady state is achieved in 36,000 seconds.

In our example, the dose rate was roughly 0.1 rads/s. Note that the dark conductivity is typically  $5 \times 10^{-16} \text{ (ohm-m)}^{-1}$ , and the RIC is therefore  $0.1 \text{ (rads/sec)} \times 3 \times 10^{-16} \text{ (sec/(ohm-m-rad))} = 0.3 \times 10^{-16} \text{ (ohm-m)}^{-1}$ . The dark conductivity dominates the response in this typical (theoretical) sample. Therefore, even if we reduced the radiation-induced conductivity (RIC) to zero, there would not be enough electric field generated in the typical sample under CRRES space radiation levels to produce any pulses.

**Table 2. Comparison of Typical FR4 Conduction Processes.**

Dark Conductivity	Radiation-Induced Conductivity
$5 \times 10^{-16} \text{ (ohm-m)}^{-1}$	$0.3 \times 10^{-16} \text{ (ohm-m)}^{-1}$

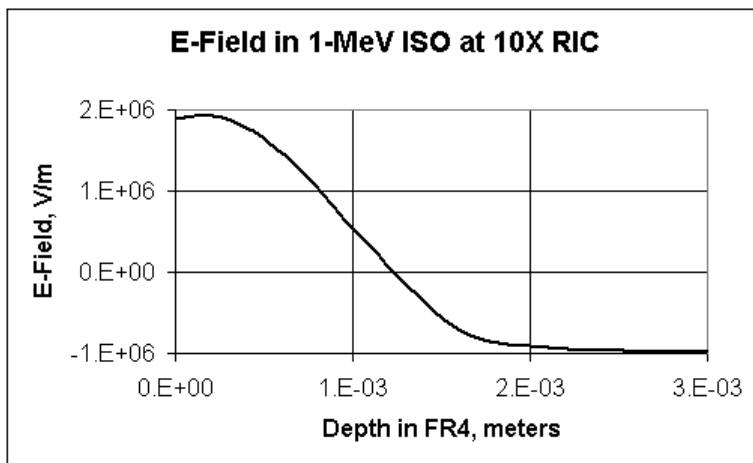


**Figure 19.** In this test, the radiation-induced conductivity (RIC) was raised a factor of ten over the “typical” FR4 value. It resulted in a slightly reduced electric field compared to that of the typical (Figure 16) FR4.

It is simply the total conductivity that bleeds away the intense electric field. This fact is exhibited in Figures 18,19 and Table 2. The test in Figure 18 altered the total conductivity by a factor of ten, and thus altered the electric field by a factor of ten. The test in Figure 19 altered the total conductivity by only 50% to produce a change of electric field by about 50%. If we have the correct values for dark conductivity and RIC for FR4, then the results in Figures 9-19 indicate that pulses are not expected during the CRRES mission from Sample 8! However, the RIC varies strongly with position whereas the dark conductivity is constant through the sample. Thus simple addition of effects may be misleading in some instances.

## Electric Fields Under Space Radiations

### *Radiation Spectra*

Perhaps there is something different in the real spectra that make larger electric fields in space. Next we estimate the electric fields in typical CRRES space spectra. The Spectra provided by the CRRES instruments have been fitted to an exponential function. The fitted spectra will be applied to Sample 8 in order to study the expected electric field strengths during the CRRES mission.

### *Typical Electric Field Calculations*

We chose to investigate the spectral dependencies possibly occurring in our test sample by comparing the electric fields generated in four cases: 1) hard, intense spectrum, 2) hard, weak spectrum, 3) soft, intense spectrum, and 4) soft, weak spectrum. These four cases are found by searching through Table 1. The four chosen spectra are listed in Table 3.

**Table 3. Representative Extreme Spectra**

Spectra Type	Spectra	Orbits
hard, intense	$A = 2.2 \times 10^{11}$ $E_0 = 0.38$	790-4
hard, weak	$A = 1.5 \times 10^{10}$ $E_0 = 0.38$	660-5
soft, intense	$A = 6.0 \times 10^{11}$ $E_0 = 0.23$	1047-50
soft, weak	$A = 1.0 \times 10^{11}$ $E_0 = 0.23$	766-70 1029-33

Typically, the chosen extreme spectra lasted about five orbits (2 days) which happens to be a little longer than the time constant for our typical FR4 sample. This is good in that our typical sample will achieve its full response to each extreme spectrum before that particular spectrum abates. On the other hand, if the actual flight sample 8 had a longer time constant (lower conductivity) than the typical sample, it will not have achieved steady state before the extreme spectrum abates. This fact should be remembered when we adjust the conductivity in computer runs later.

The extreme spectra produce the following dose rates and current penetrations. Figure 20 shows a dose rate in the traditional plot, and Figure 21 shows all four dose-rates in a logarithmic plot. Figure 22 shows the four spectra current penetrations (absolute value) in a logarithmic plot.

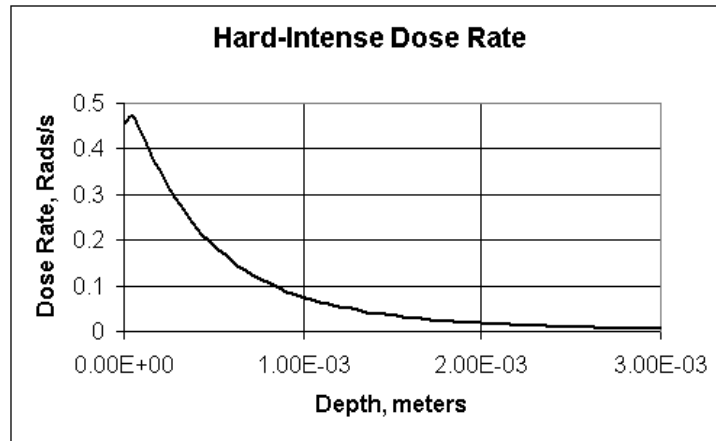


**Figure 20. Dose Rate for the Hard Intense Spectrum.**

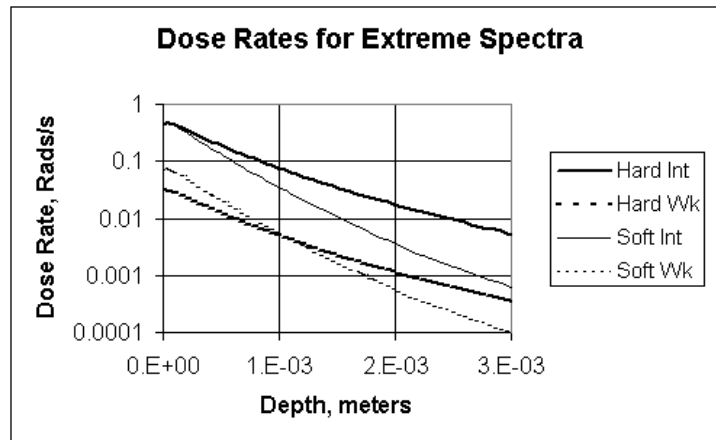


**Figure 21. Dose Rates for All Four Extreme Spectra.**

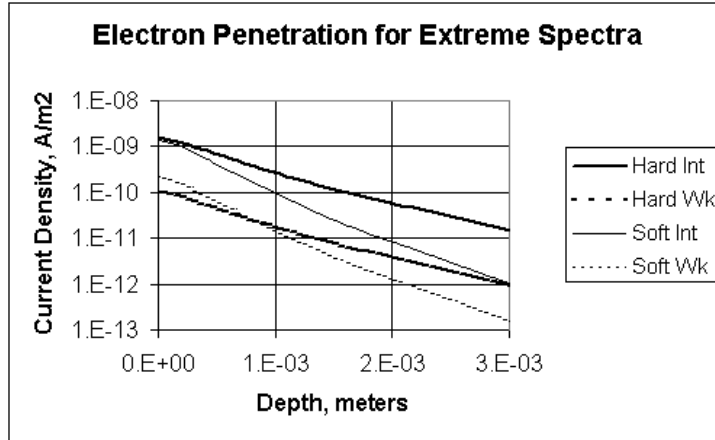


**Figure 22. Electron Current Penetration for All Four Extreme Spectra.**

Figures 23-26 show the electric field in the typical sample 8 after 180,000 seconds (ten half-orbits or 50 hours) under each spectrum. Each of the four runs began with no electric field.

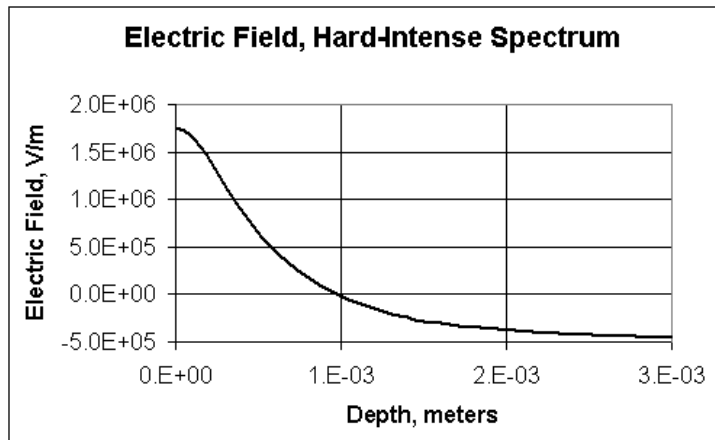


**Figure 23. Steady State Electric Field in Typical Sample 8 by Hard-Intense Spectrum in Table 3.**

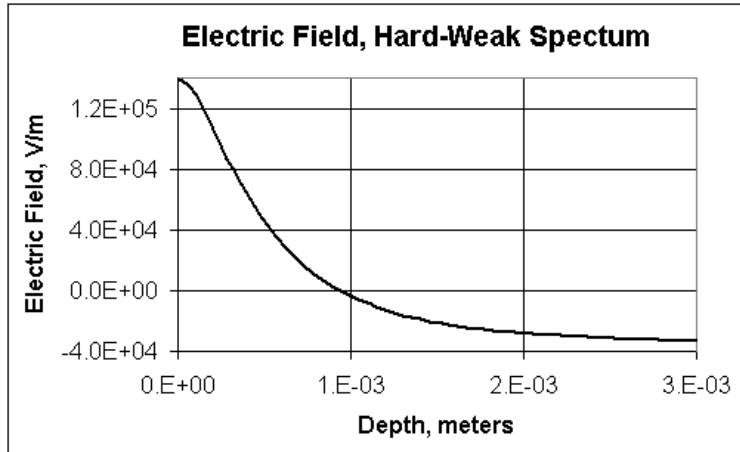


**Figure 24. Steady State Electric Field in Typical Sample 8 by Hard-Weak Spectrum in Table 3.**

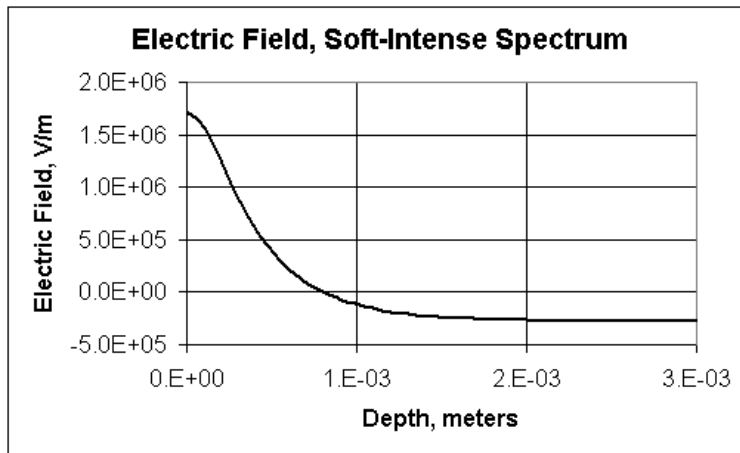


**Figure 25. Steady State Electric Field in Typical Sample 8 by Soft-Intense Spectrum in Table 3.**

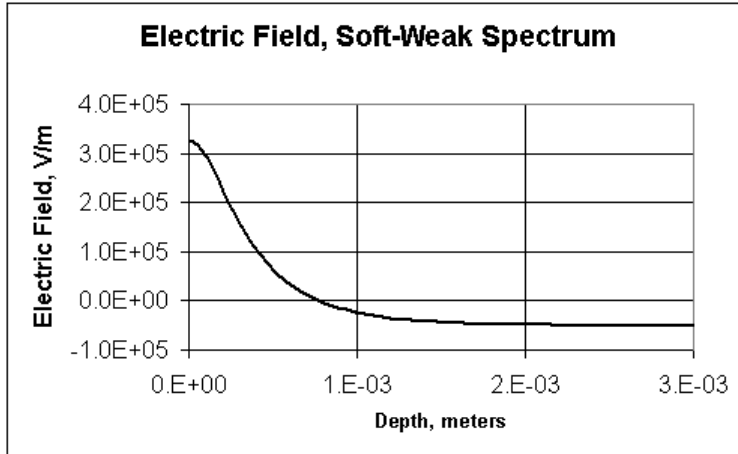


**Figure 26. Steady State Electric Field in Typical Sample 8 by Soft-Weak Spectrum in Table 3.**

It is difficult to inter-compare Figures 23-26 because both parameters, “A” and  $E_0$ , were seemingly random. For example, the soft-intense spectrum is much more intense than is the hard-intense spectrum because that is what happened in space. But the four figures do exhibit the spectral effects that are clearly seen in Figures 6-7. That is because harder spectra produce larger electric field (for similar A), and more intense spectra also produce larger electric field (for similar  $E_0$ ).

The plots of dose rate and high-energy electron current in Figures 20-22 demonstrate that in neither case did much dose penetrate to the rear of the sample. Therefore, dark conductivity in the typical sample provides all of the leakage in the rear of the sample. Furthermore, the dark conductivity is larger than the RIC everywhere in the sample for any spectrum.

The plots of electric field for the four extreme spectra do not show electric field amplitudes sufficient to produce pulses. The dark conduction is bleeding away the charge before the electric field can achieve significant amplitude. If the extreme spectra do not produce pulsing, it seems unlikely that more typical spectra will generate pulsing either.

### 2.3 Theoretical Determination of Conductivity in FR4 in Space

#### The Third Study:

*In the third study, we propose to use NUMIT for estimating a range of validity for the dark resistivity in the IDM FR4 insulator.*

#### Conductivity in Space

In order to produce pulses, it is necessary to achieve about  $1 \times 10^7$  V/m in the insulator. Our calculations failed to provide such electric field strength for the “Typical” FR4 material. But we note that the material did not pulse for the first half (550 orbits) of the CRRES mission. Perhaps

for the early part of the mission, the electric fields were close to our computer predictions for the typical sample.

Figures 11-12 and Table 1 indicate the effects of varying the two conductivities, dark and RIC. Decreasing the RIC would not alter the electric fields to any significant degree. Only by decreasing the dark conductivity relative to the typical value would larger electric field be achieved, large enough to produce pulsing.

The radiation-induced conductivity in FR4 is given by  $\sigma = k_p R^\Delta$ . The coefficient,  $k_p$  is here assumed to be  $3 \times 10^{-16}$  (s/ohm-m-rad) from [3]. The exponent,  $\Delta$ , usually lies between 0.5 and 1.0, typically close to 1.0 at our dose rates. These values are used in our work here as “typical” values, and will continue to be used since we have no evidence to the contrary.

The dark conductivity current is given by a conductivity coefficient,  $\sigma$ , times the electric field. Conductivity,  $\sigma$ , of the FR4 sample is herein initially estimated from the charge decay time constant recently measured on another FR4 sample. Figure 12 in [5] shows that the un-irradiated FR4 charged-surface decayed by  $1/e$  in about one day. The conductivity,  $\sigma$ , is therefore initially assumed to be  $5 \times 10^{-16}$  (ohm-m)<sup>-1</sup>. This conductivity is called the “typical” conductivity of our sample, and was used to develop the data in some of the prior Figs.

Evidence in [6] and the results from CRRES/IDM indicate that the dark conductivity in FR4 decreases perhaps by an order of magnitude after high-energy irradiation. It has been well established that TFE Teflon increases its conductivity with irradiation both on CRRES/IDM [1] and in ground testing [7]. FR4 seems to be different from TFE Teflon as [1] also indicates. Therefore, both the typical and the improved values listed in Table 3 will be used to attempt to predict the pulsing history of sample 8 on the CRRES/IDM experiment.

**Table 4. Typical and Improved FR4 Conduction Processes.**

Dark Conductivity	Radiation-Induced Conductivity
<b>typical</b> = $5 \times 10^{-16}$ (ohm-m) <sup>-1</sup>	<b>typical</b> = $0.3 \times 10^{-16}$ (ohm-m) <sup>-1</sup>
<b>improved</b> $5 \times 10^{-17}$	<b>“improved”</b> same as typical

The result of using NUMIT with the conductivity terms in Table 4 for the orbits starting at 590 to the end of mission, orbit 1067, are shown in Figure 27.

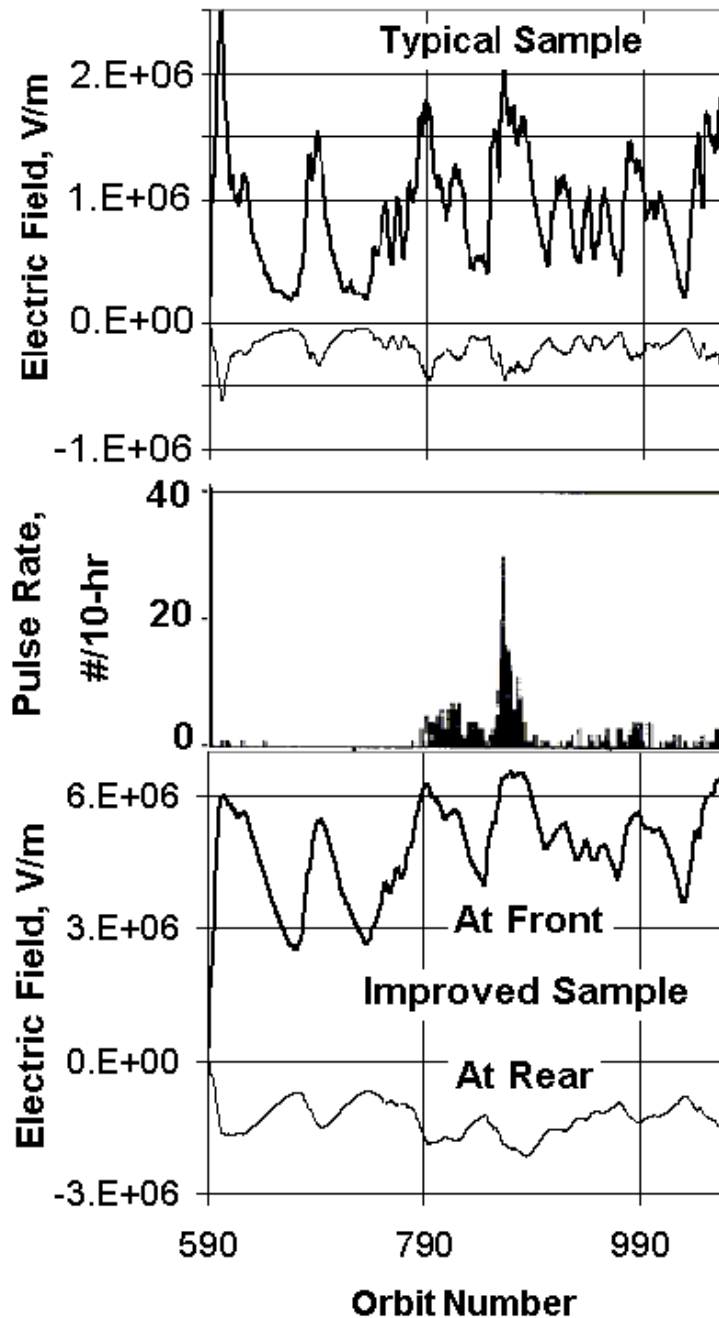


**Figure 27. Calculated Electric Field Strengths at the Front and Rear of Sample 8 During the Mission for Two Sets of Parameters, Compared to Pulsing During the Mission.**

For the assumed parameter values, neither case generates an electric field as large as  $1 \times 10^7$  V/m. But the improved sample values in Table 4 come close to generating such field strength. Decreasing the conductivity by another factor 1/3, as in Table 5, probably would achieve the goal. However, consider the following.

Note that the improved sample response predicted in Figure 27 has the largest electric field at a time (near orbit 870) when the in-space pulsing was most frequent. So at least we have come closer to the proper values for in-space conductivity. The “typical” sample shown in the top graph generates the largest electric field strength around orbit 600. But this electric field is not very strong.

With these improved values, the RIC is approaching a magnitude similar to the dark conductivity. One could adjust either conductivity parameter to produce the necessary further improvement in the correlation between predicted electric field and pulse rate per orbit. So, we stop here, making the last adjustment to the dark conductivity as shown in Table 5. Since we now possess sister-samples of the original sample 8, we can measure the dark conductivity in the lab using the newest methods. There is no need to continue guessing any further.

**Table 5. First Guess at Best FR4 Conduction Processes.**

Dark Conductivity	Radiation-Induced Conductivity
<b>typical</b> = $5 \times 10^{-16}$ (ohm-m) <sup>-1</sup>	<b>typical</b> = $0.3 \times 10^{-16}$ (ohm-m) <sup>-1</sup>
<b>improved</b> $5 \times 10^{-17}$	<b>“improved”</b> same as typical
<b>best guess</b> $1.7 \times 10^{-17}$	<b>best guess</b> same as typical

The purpose of this section on the “Third Study” is to use all FR4 pulsing data in order to attempt to find a best value for conductivity. From the results already discussed, it would not be meaningful to do this now. Figure 5a shows how all FR4 samples behaved. Note that the other samples, having floating front surfaces, produced many pulses around orbit 600, unlike sample 8. This fact tells us that we need to know how to distinguish pulsing with a floating surface from that of a grounded surface. Another mechanism must be happening.

The fact of a floating front surface has been discussed in controlled laboratory experiments [9]. It cannot be secondary electron emission alone that explains the electric field developments at a floating surface compared to a grounded one. The floating surface also emits electrons depending on the dose rate and field inside the insulator near the surface [5]. But we don’t have quantitative knowledge of these emissions. Also, the pulse-discharge mechanism is different when a floating surface is involved, and larger pulses are seen with floating surfaces. Perhaps the detectors counted more pulses from floating surfaces because the grounded-surface pulses were borderline for the pulse detector. Because we cannot explain the pulsing near orbit 600 by the other FR4 samples, we would be foolish to attempt to use the data to further improve our estimate of conductivity in FR4.

There is one piece of information that is available from a comparison between the thin sample with floating surface (#15) and the two otherwise-similar thick samples with floating surface. (#4,12) in Figure 5a. The thin sample has a larger dose rate at the rear electrode, yet most of the high-energy electrons are stopped in the sample. It is probably correct to say that the RIC at the rear of the thin sample is providing measurable increased conduction relative to the dark

conduction. Figure 20 shows the level of dose at the rear (.119 cm) of sample 15, roughly 0.03 rads/second during periods of pulsing. For it to have effect relative to dark conduction, the order of magnitude for the RIC coefficient,  $k_p$ , must be not far from that listed in Table 5.

### 3. Conclusions

Due to the “success” as shown in Figure 27, being able to predict electric field in correspondence with pulsing during a space flight is a “first”. Eventually, one may get good enough at this kind of analysis to be able to predict pulse rates on critical systems to show that the rate is less than a predetermined maximum allowable number of pulses per mission lifetime. This would be a big improvement over the present practice of attempting to put everything into Faraday cages, and keeping our fingers crossed that nothing goes zap inside those cages.

The study was also a success in relating flux and hardness of spectra to the pulse rate and electric field. It gives further credence to the high-energy electron spectral data provided by the CRRES instruments. Setting the electron spectrum constant during each half-orbit is successful only because the time constant of the FR4 is much longer than a half-orbit duration. We gambled that all of the diverse data sets could be brought together into a code like NUMIT and produce reasonable answers.

This study has found that FR4 dark conductivity is much less than handbook values indicate, but of the order that recent studies have measured using an improved technique [5]. The RIC is of the order of those in the literature, but perhaps an improved measurement should be performed for FR4. Since other materials have even less conductivity (Kapton PCB for example), they should be evaluated for pulsing at even lower radiation flux.

The NUMIT method seems to work but it is limited to cases with known surface voltage. The mechanisms of charging of samples with floating surfaces need to be determined if such pulsing is to be understood and predicted.

In the process of performing this work, a simple method to analytically determine the dose-depth and charge-current profile for isotropic radiations was discovered. This might have advantages in determining dose-depth in spacecraft compared to the expensive Monte-Carlo transport methods. Perhaps one might attempt to generalize the method in the future.

One might develop a dosimeter based on pulsing rate. Perhaps a material can be made that reliably pulses at a rate functionally proportional to radiation flux. It is simple to count pulses, and the data is immediately a digital number requiring no conversion from an analytical form.

## 4. References

- [1] A. R. Frederickson, E. G. Holeman and E. G. Mullen, "Characteristics of Spontaneous Electrical Discharging of Various Insulators in Space Radiations," *IEEE Trans. Nuc. Sci.* **39**, 1773-82, 1992.
- [2] A. R. Frederickson, E. G. Mullen, K. J. Kerns and P. A. Robinson, "The CRRES IDM Spacecraft Experiment for Insulator Discharge Pulses," *IEEE Transactions on Nuclear Science*, **40**, No. 2, 233-41, 1993.
- [3] A. R. Frederickson, "Radiation Induced Currents and Conductivity in Dielectrics", *IEEE Trans. Nuc. Sci NS24*, 2532-9, 1977.
- [4] A. R. Frederickson, C. E. Benson and J. F. Bockman, "Measurement of Charge Storage and Leakage in Polyimides," *Nuclear Instruments and Methods in Physics Research B*, 454-60, 2003.
- [5] A. R. Frederickson and J. R. Dennison, "Measurement of Conductivity and Charge Storage in Insulators Related to Spacecraft Charging," accepted for publication in *IEEE Trans. Nuc. Sci.*, December, 2003.
- [6] A. R. Frederickson A. C. Whittlesey and H. B. Garrett, "Comparing CRRES Internal Discharge Monitor Results With Ground Tests And Published Guidelines," *Proceedings, Seventh Spacecraft Charging Technology Conference, Noordwijk, Netherlands, May, 2001.*
- [7] A. R. Frederickson, "Irradiation Effects on Charge Storage in Teflon", *Proceedings 1981 Conference on Electrical Insulation and Dielectric Phenomena*, pp. 45-51, *IEEE Publ # 81 CH1668-3* (1981).
- [8] A. R. Frederickson, "New Scaling Laws for Spacecraft Discharge Pulses," *Proceedings, Seventh Spacecraft Charging Technology Conference, Noordwijk, Netherlands, May, 2001.*
- [9] A. R. Frederickson, "Concepts for Secondary Electron Emission from Irradiated Insulators," *Proceedings XVII International Symposium on Discharges and Electrical Insulation in Vacuum*, 517-22, July 1996, *IEEE*, 445 Hoes Lane, Piscataway, NJ, USA, #96CH35939, ISBN 0-7803-2906-6.
- [10] Vampola, A.L., J.V. Osborn, and B.M. Johnson, "CRRES magnetic electron spectrometer AFGL-701-5A (MEA)," *J. Spacecr. Rockets*, **29**, 592-595, 1992.
- [11] Dichter, B.K., Hanser, F.A., Sellers, B., Hunerwadel, J.L., "High Energy Electron Fluxmeter," *IEEE Transactions on Nuclear Science* **40**, No. 2, 242-245, 1993.

## 5. Acknowledgements

Thanks to Robin Evans for assistance with the Fortran in the NUMIT code, and to Insoo Jun for providing MCNP Monte-Carlo transport data for dose-depth and current-depth.

## 6. Appendix

Table 1 provides tabulation of the parameter fits to half-orbit spectra data from orbits 590 through 1066.

orbit	A	$E_0$	Corr Coeff
590.0	2.752E+10	0.238	0.931
590.5	1.973E+11	0.238	0.972
591.0	2.125E+11	0.232	0.979
591.5	3.181E+11	0.221	0.981
592.0	6.161E+11	0.230	0.998
592.5	5.077E+11	0.274	0.994
593.0	3.200E+11	0.273	0.994
593.5	2.089E+11	0.251	0.998
594.0	2.270E+11	0.286	0.997
594.5	2.638E+11	0.271	0.995
595.0	3.626E+11	0.276	0.998
595.5	3.555E+11	0.301	0.995
596.0	3.165E+11	0.300	0.995
596.5	3.753E+11	0.269	0.996
597.0	5.822E+11	0.285	0.998
597.5	5.560E+11	0.321	0.997
598.0	4.308E+11	0.323	0.996
598.5	3.574E+11	0.308	0.998
599.0	4.186E+11	0.343	0.997
599.5	3.733E+11	0.362	0.998
600.0	3.668E+11	0.369	0.997
600.5	3.318E+11	0.360	0.998
601.0	2.955E+11	0.359	0.998
601.5	2.494E+11	0.349	0.998
602.0	2.827E+11	0.358	0.997
602.5	2.711E+11	0.351	0.997
603.0	2.052E+11	0.325	0.000
603.5	1.662E+11	0.305	0.997
604.0	2.014E+11	0.311	0.997
604.5	2.283E+11	0.321	0.997
605.0	2.182E+11	0.326	0.997
605.5	1.706E+11	0.331	0.997
606.0	1.682E+11	0.341	0.997
606.5	1.293E+11	0.332	0.996
607.0	1.242E+11	0.335	0.997
607.5	1.306E+11	0.340	0.996
608.0	1.029E+11	0.335	0.995
608.5	8.410E+10	0.329	0.993
609.0	1.367E+11	0.337	0.994
609.5	1.547E+11	0.341	0.000
610.0	1.629E+11	0.341	0.995
610.5	1.663E+11	0.337	0.000
611.0	1.672E+11	0.332	0.995
611.5	1.649E+11	0.331	0.000
612.0	1.537E+11	0.330	0.996
612.5	1.242E+11	0.328	0.000
613.0	1.040E+11	0.326	0.988
613.5	1.139E+11	0.327	0.000
614.0	1.301E+11	0.328	0.989
614.5	1.452E+11	0.329	0.000
615.0	1.499E+11	0.328	0.994
615.5	1.316E+11	0.323	0.000
616.0	1.168E+11	0.316	0.991
616.5	1.218E+11	0.310	0.000
617.0	1.298E+11	0.308	0.989
617.5	1.349E+11	0.315	0.000
618.0	1.468E+11	0.317	0.990
618.5	1.756E+11	0.307	0.000
619.0	1.953E+11	0.300	0.992
619.5	1.858E+11	0.309	0.000
620.0	1.794E+11	0.316	0.992
620.5	1.943E+11	0.312	0.000
621.0	2.092E+11	0.306	0.992
621.5	2.132E+11	0.303	0.000
622.0	2.066E+11	0.301	0.991
622.5	1.812E+11	0.302	0.000
623.0	1.648E+11	0.302	0.992
623.5	1.778E+11	0.300	0.000
624.0	1.835E+11	0.298	0.993
624.5	1.578E+11	0.302	0.000
625.0	1.353E+11	0.306	0.991
625.5	1.354E+11	0.307	0.000
626.0	1.362E+11	0.308	0.993
626.5	1.270E+11	0.312	0.000
627.0	1.114E+11	0.319	0.992
627.5	8.618E+10	0.329	0.000
628.0	6.863E+10	0.334	0.992
628.5	7.303E+10	0.328	0.000
629.0	7.634E+10	0.325	0.991
629.5	6.620E+10	0.335	0.000
630.0	6.018E+10	0.344	0.990
630.5	7.014E+10	0.345	0.000
631.0	7.913E+10	0.344	0.991
631.5	7.799E+10	0.342	0.000
632.0	7.470E+10	0.341	0.990
632.5	7.161E+10	0.345	0.000
633.0	6.879E+10	0.350	0.991
633.5	6.644E+10	0.355	0.000
634.0	6.207E+10	0.360	0.993
634.5	5.294E+10	0.367	0.000
635.0	4.627E+10	0.371	0.992
635.5	4.754E+10	0.370	0.000
636.0	4.905E+10	0.369	0.991
636.5	4.714E+10	0.372	0.000

637.0	4.583E+10	0.374	0.991
637.5	4.760E+10	0.374	0.000
638.0	4.999E+10	0.373	0.991
638.5	5.226E+10	0.371	0.000
639.0	5.190E+10	0.371	0.992
639.5	4.571E+10	0.372	0.000
640.0	3.991E+10	0.374	0.992
640.5	3.792E+10	0.375	0.000
641.0	3.646E+10	0.376	0.993
641.5	3.430E+10	0.378	0.000
642.0	3.312E+10	0.380	0.991
642.5	3.453E+10	0.379	0.000
643.0	3.618E+10	0.377	0.992
643.5	3.705E+10	0.377	0.000
644.0	3.652E+10	0.377	0.991
644.5	3.321E+10	0.382	0.000
645.0	3.018E+10	0.385	0.991
645.5	2.920E+10	0.383	0.000
646.0	2.812E+10	0.381	0.990
646.5	2.576E+10	0.382	0.000
647.0	2.389E+10	0.383	0.990
647.5	2.377E+10	0.381	0.000
648.0	2.380E+10	0.381	0.983
648.5	2.327E+10	0.382	0.000
649.0	2.329E+10	0.381	0.987
649.5	2.483E+10	0.375	0.000
650.0	2.652E+10	0.370	0.981
650.5	2.780E+10	0.369	0.000
651.0	2.812E+10	0.368	0.982
651.5	2.652E+10	0.367	0.000
652.0	2.559E+10	0.367	0.970
652.5	2.717E+10	0.367	0.000
653.0	2.813E+10	0.367	0.975
653.5	2.645E+10	0.369	0.000
654.0	2.508E+10	0.370	0.975
654.5	2.578E+10	0.369	0.000
655.0	2.677E+10	0.369	0.975
655.5	2.741E+10	0.369	0.000
656.0	2.664E+10	0.370	0.977
656.5	2.292E+10	0.373	0.000
657.0	1.997E+10	0.376	0.979
657.5	2.025E+10	0.377	0.000
658.0	2.026E+10	0.380	0.980
658.5	1.809E+10	0.386	0.000
659.0	1.683E+10	0.388	0.979
659.5	1.874E+10	0.380	0.000
660.0	2.066E+10	0.373	0.976
660.5	2.102E+10	0.373	0.000
661.0	2.048E+10	0.375	0.976
661.5	1.867E+10	0.378	0.000
662.0	1.677E+10	0.381	0.975
662.5	1.528E+10	0.385	0.000
663.0	1.460E+10	0.386	0.980
663.5	1.555E+10	0.380	0.000

664.0	1.640E+10	0.375	0.970
664.5	1.620E+10	0.380	0.000
665.0	1.667E+10	0.380	0.974
665.5	1.912E+10	0.368	0.000
666.0	2.320E+10	0.356	0.963
666.5	2.993E+10	0.350	0.000
667.0	3.581E+10	0.346	0.970
667.5	3.844E+10	0.346	0.000
668.0	3.737E+10	0.348	0.974
668.5	2.959E+10	0.354	0.000
669.0	2.241E+10	0.361	0.973
669.5	1.989E+10	0.367	0.000
670.0	1.997E+10	0.367	0.975
670.5	2.353E+10	0.356	0.000
671.0	2.894E+10	0.344	0.966
671.5	3.679E+10	0.334	0.000
672.0	4.898E+10	0.325	0.979
672.5	6.974E+10	0.316	0.000
673.0	8.091E+10	0.312	0.982
673.5	6.624E+10	0.318	0.000
674.0	5.534E+10	0.323	0.981
674.5	6.585E+10	0.320	0.000
675.0	7.517E+10	0.315	0.983
675.5	7.106E+10	0.310	0.000
676.0	7.249E+10	0.304	0.983
676.5	9.307E+10	0.296	0.000
677.0	1.269E+11	0.289	0.983
677.5	1.809E+11	0.286	0.000
678.0	2.157E+11	0.285	0.990
678.5	1.968E+11	0.287	0.000
679.0	1.910E+11	0.291	0.995
679.5	2.416E+11	0.295	0.000
680.0	2.748E+11	0.298	0.998
680.5	2.408E+11	0.301	0.000
681.0	2.151E+11	0.304	0.997
681.5	2.414E+11	0.310	0.000
682.0	2.536E+11	0.314	0.998
682.5	2.082E+11	0.312	0.000
683.0	1.609E+11	0.309	0.993
683.5	1.381E+11	0.304	0.000
684.0	1.414E+11	0.300	0.993
684.5	1.914E+11	0.301	0.000
685.0	2.273E+11	0.302	0.996
685.5	2.082E+11	0.304	0.000
686.0	1.987E+11	0.307	0.995
686.5	2.385E+11	0.311	0.000
687.0	2.710E+11	0.315	0.997
687.5	2.625E+11	0.316	0.000
688.0	2.494E+11	0.316	0.998
688.5	2.461E+11	0.316	0.000
689.0	2.448E+11	0.317	0.000
689.5	2.432E+11	0.319	0.000
690.0	2.287E+11	0.321	0.998
690.5	1.856E+11	0.320	0.000

691.0	1.581E+11	0.320	0.998
691.5	1.803E+11	0.325	0.000
692.0	1.971E+11	0.330	0.998
692.5	1.770E+11	0.331	0.000
693.0	1.539E+11	0.332	0.998
693.5	1.424E+11	0.335	0.000
694.0	1.380E+11	0.338	0.998
694.5	1.434E+11	0.339	0.000
695.0	1.394E+11	0.341	0.998
695.5	1.089E+11	0.342	0.000
696.0	8.677E+10	0.343	0.997
696.5	9.668E+10	0.345	0.000
697.0	1.043E+11	0.345	0.998
697.5	9.085E+10	0.341	0.000
698.0	7.861E+10	0.340	0.997
698.5	7.969E+10	0.342	0.000
699.0	8.365E+10	0.345	0.997
699.5	8.741E+10	0.345	0.000
700.0	8.657E+10	0.345	0.997
700.5	7.543E+10	0.345	0.000
701.0	6.643E+10	0.343	0.996
701.5	6.735E+10	0.341	0.000
702.0	6.691E+10	0.337	0.992
702.5	5.843E+10	0.333	0.000
703.0	5.286E+10	0.331	0.994
703.5	5.791E+10	0.334	0.000
704.0	6.310E+10	0.337	0.993
704.5	6.331E+10	0.337	0.000
705.0	5.998E+10	0.337	0.993
705.5	5.116E+10	0.340	0.000
706.0	4.554E+10	0.342	0.993
706.5	4.988E+10	0.342	0.000
707.0	5.196E+10	0.341	0.994
707.5	4.400E+10	0.341	0.000
708.0	3.814E+10	0.341	0.993
708.5	4.204E+10	0.342	0.000
709.0	4.551E+10	0.343	0.993
709.5	4.316E+10	0.340	0.000
710.0	3.858E+10	0.338	0.992
710.5	3.191E+10	0.337	0.000
711.0	2.737E+10	0.334	0.989
711.5	2.870E+10	0.323	0.000
712.0	2.937E+10	0.314	0.977
712.5	2.563E+10	0.309	0.000
713.0	2.560E+10	0.304	0.974
713.5	3.610E+10	0.296	0.000
714.0	4.528E+10	0.290	0.979
714.5	4.619E+10	0.289	0.000
715.0	4.641E+10	0.289	0.977
715.5	4.918E+10	0.286	0.000
716.0	5.390E+10	0.283	0.975
716.5	6.175E+10	0.279	0.000
717.0	6.410E+10	0.278	0.982
717.5	5.253E+10	0.282	0.000

718.0	4.557E+10	0.286	0.980
718.5	5.591E+10	0.288	0.000
719.0	6.654E+10	0.289	0.984
719.5	6.920E+10	0.290	0.000
720.0	6.632E+10	0.288	0.000
720.5	5.496E+10	0.282	0.000
721.0	4.560E+10	0.278	0.967
721.5	4.498E+10	0.278	0.000
722.0	4.345E+10	0.281	0.967
722.5	3.551E+10	0.287	0.000
723.0	3.079E+10	0.291	0.965
723.5	3.652E+10	0.291	0.000
724.0	4.035E+10	0.290	0.965
724.5	3.464E+10	0.288	0.000
725.0	3.090E+10	0.288	0.974
725.5	3.632E+10	0.292	0.000
726.0	4.160E+10	0.294	0.969
726.5	4.200E+10	0.294	0.000
727.0	4.038E+10	0.294	0.973
727.5	3.671E+10	0.295	0.000
728.0	3.531E+10	0.297	0.972
728.5	4.007E+10	0.297	0.000
729.0	4.209E+10	0.298	0.973
729.5	3.487E+10	0.301	0.000
730.0	2.979E+10	0.304	0.972
730.5	3.411E+10	0.307	0.000
731.0	3.740E+10	0.310	0.971
731.5	3.366E+10	0.313	0.000
732.0	2.882E+10	0.316	0.977
732.5	2.500E+10	0.320	0.000
733.0	2.241E+10	0.323	0.975
733.5	2.206E+10	0.324	0.000
734.0	2.146E+10	0.324	0.973
734.5	1.913E+10	0.325	0.000
735.0	2.245E+10	0.323	0.971
735.5	3.933E+10	0.314	0.000
736.0	5.080E+10	0.308	0.971
736.5	4.331E+10	0.308	0.000
737.0	4.091E+10	0.307	0.969
737.5	5.946E+10	0.300	0.000
738.0	7.498E+10	0.294	0.976
738.5	7.318E+10	0.296	0.000
739.0	6.813E+10	0.298	0.979
739.5	6.439E+10	0.299	0.000
740.0	7.852E+10	0.298	0.976
740.5	1.322E+11	0.294	0.000
741.0	1.644E+11	0.292	0.986
741.5	1.286E+11	0.296	0.000
742.0	9.030E+10	0.300	0.983
742.5	8.074E+10	0.302	0.000
743.0	7.835E+10	0.302	0.000
743.5	7.775E+10	0.302	0.000
744.0	8.017E+10	0.302	0.000
744.5	8.847E+10	0.302	0.000

745.0	9.568E+10	0.302	0.986
745.5	9.748E+10	0.302	0.000
746.0	9.368E+10	0.302	0.000
746.5	8.000E+10	0.303	0.000
747.0	7.924E+10	0.302	0.987
747.5	1.125E+11	0.300	0.000
748.0	1.418E+11	0.297	0.990
748.5	1.448E+11	0.292	0.000
749.0	1.407E+11	0.289	0.990
749.5	1.332E+11	0.290	0.000
750.0	1.428E+11	0.292	0.992
750.5	1.924E+11	0.292	0.000
751.0	2.171E+11	0.293	0.997
751.5	1.658E+11	0.295	0.000
752.0	1.271E+11	0.297	0.993
752.5	1.544E+11	0.302	0.000
753.0	1.789E+11	0.304	0.997
753.5	1.641E+11	0.301	0.000
754.0	1.347E+11	0.298	0.996
754.5	9.191E+10	0.298	0.000
755.0	6.323E+10	0.297	0.976
755.5	7.291E+10	0.292	0.000
756.0	7.897E+10	0.289	0.977
756.5	5.770E+10	0.290	0.000
757.0	4.489E+10	0.290	0.965
757.5	6.474E+10	0.288	0.000
758.0	7.868E+10	0.287	0.982
758.5	6.300E+10	0.288	0.000
759.0	6.367E+10	0.289	0.970
759.5	1.159E+11	0.288	0.000
760.0	1.705E+11	0.285	0.987
760.5	2.045E+11	0.279	0.000
761.0	2.136E+11	0.275	0.993
761.5	1.769E+11	0.275	0.000
762.0	1.667E+11	0.276	0.989
762.5	2.387E+11	0.274	0.000
763.0	2.818E+11	0.273	0.997
763.5	2.188E+11	0.277	0.000
764.0	1.579E+11	0.283	0.991
764.5	1.548E+11	0.291	0.000
765.0	1.508E+11	0.297	0.995
765.5	1.159E+11	0.295	0.000
766.0	8.087E+10	0.289	0.986
766.5	6.096E+10	0.278	0.000
767.0	5.511E+10	0.266	0.967
767.5	7.329E+10	0.255	0.000
768.0	9.650E+10	0.242	0.960
768.5	1.190E+11	0.224	0.000
769.0	1.540E+11	0.215	0.985
769.5	2.173E+11	0.227	0.000
770.0	2.505E+11	0.240	0.971
770.5	2.020E+11	0.244	0.000
771.0	1.704E+11	0.244	0.970
771.5	2.182E+11	0.240	0.000

772.0	3.003E+11	0.236	0.976
772.5	4.200E+11	0.232	0.000
773.0	4.849E+11	0.228	0.995
773.5	4.079E+11	0.225	0.000
774.0	3.297E+11	0.226	0.990
774.5	3.198E+11	0.237	0.000
775.0	3.021E+11	0.246	0.990
775.5	2.331E+11	0.244	0.000
776.0	1.852E+11	0.244	0.979
776.5	2.108E+11	0.253	0.000
777.0	2.561E+11	0.257	0.996
777.5	3.088E+11	0.243	0.000
778.0	3.209E+11	0.232	0.998
778.5	2.376E+11	0.235	0.000
779.0	1.773E+11	0.248	0.981
779.5	2.164E+11	0.277	0.000
780.0	2.419E+11	0.296	0.997
780.5	1.871E+11	0.284	0.000
781.0	1.783E+11	0.270	0.979
781.5	3.128E+11	0.264	0.000
782.0	4.171E+11	0.259	0.988
782.5	3.813E+11	0.251	0.000
783.0	3.431E+11	0.253	0.998
783.5	3.693E+11	0.277	0.000
784.0	3.717E+11	0.306	0.998
784.5	2.885E+11	0.333	0.000
785.0	2.085E+11	0.348	0.995
785.5	1.787E+11	0.338	0.000
786.0	1.718E+11	0.326	0.989
786.5	2.149E+11	0.329	0.993
787.0	2.794E+11	0.347	0.992
787.5	2.527E+11	0.348	0.995
788.0	1.889E+11	0.327	0.995
788.5	2.043E+11	0.338	0.994
789.0	2.687E+11	0.366	0.995
789.5	2.575E+11	0.362	0.995
790.0	1.892E+11	0.340	0.997
790.5	1.718E+11	0.348	0.994
791.0	2.143E+11	0.370	0.995
791.5	2.324E+11	0.375	0.996
792.0	2.145E+11	0.374	0.994
792.5	1.783E+11	0.370	0.995
793.0	1.610E+11	0.360	0.995
793.5	1.794E+11	0.365	0.996
794.0	2.051E+11	0.380	0.994
794.5	1.821E+11	0.367	0.994
795.0	1.292E+11	0.343	0.994
795.5	1.195E+11	0.349	0.994
796.0	1.427E+11	0.363	0.995
796.5	1.264E+11	0.354	0.994
797.0	1.176E+11	0.334	0.994
797.5	1.159E+11	0.336	0.995
798.0	1.368E+11	0.347	0.993
798.5	1.489E+11	0.346	0.000

799.0	1.474E+11	0.348	0.994
799.5	1.221E+11	0.354	0.993
800.0	1.067E+11	0.347	0.994
800.5	1.318E+11	0.343	0.994
801.0	1.810E+11	0.340	0.992
801.5	1.721E+11	0.333	0.992
802.0	1.204E+11	0.328	0.992
802.5	1.337E+11	0.336	0.993
803.0	1.786E+11	0.344	0.993
803.5	1.605E+11	0.343	0.992
804.0	1.238E+11	0.337	0.993
804.5	1.101E+11	0.340	0.992
805.0	1.248E+11	0.343	0.992
805.5	1.310E+11	0.343	0.993
806.0	1.275E+11	0.344	0.990
806.5	9.195E+10	0.345	0.993
807.0	8.442E+10	0.343	0.990
807.5	1.022E+11	0.348	0.992
808.0	1.296E+11	0.348	0.991
808.5	1.084E+11	0.348	0.992
809.0	6.192E+10	0.349	0.992
809.5	8.019E+10	0.341	0.990
810.0	1.508E+11	0.327	0.989
810.5	1.539E+11	0.326	0.988
811.0	1.086E+11	0.332	0.990
811.5	1.119E+11	0.332	0.990
812.0	1.616E+11	0.325	0.993
812.5	1.960E+11	0.323	0.000
813.0	2.090E+11	0.324	0.995
813.5	1.727E+11	0.325	0.995
814.0	1.300E+11	0.327	0.994
814.5	1.577E+11	0.332	0.994
815.0	2.203E+11	0.332	0.996
815.5	1.970E+11	0.330	0.995
816.0	1.176E+11	0.330	0.993
816.5	1.282E+11	0.341	0.994
817.0	1.967E+11	0.341	0.996
817.5	1.958E+11	0.340	0.996
818.0	1.390E+11	0.338	0.995
818.5	1.208E+11	0.342	0.994
819.0	1.498E+11	0.341	0.996
819.5	1.705E+11	0.343	0.996
820.0	1.681E+11	0.344	0.997
820.5	1.267E+11	0.351	0.996
821.0	9.539E+10	0.353	0.994
821.5	1.182E+11	0.353	0.995
822.0	1.612E+11	0.352	0.997
822.5	1.421E+11	0.349	0.997
823.0	8.645E+10	0.345	0.995
823.5	9.386E+10	0.350	0.996
824.0	1.274E+11	0.360	0.997
824.5	1.150E+11	0.371	0.997
825.0	6.946E+10	0.374	0.997
825.5	5.354E+10	0.374	0.992

826.0	5.090E+10	0.369	0.991
826.5	4.863E+10	0.362	0.990
827.0	6.108E+10	0.355	0.985
827.5	5.806E+10	0.353	0.985
828.0	5.411E+10	0.332	0.982
828.5	7.896E+10	0.306	0.991
829.0	8.958E+10	0.324	0.988
829.5	8.003E+10	0.325	0.991
830.0	4.669E+10	0.326	0.983
830.5	5.095E+10	0.311	0.994
831.0	5.877E+10	0.347	0.987
831.5	5.023E+10	0.357	0.983
832.0	3.671E+10	0.360	0.985
832.5	3.542E+10	0.366	0.977
833.0	4.491E+10	0.358	0.980
833.5	4.797E+10	0.355	0.980
834.0	4.717E+10	0.355	0.000
834.5	4.226E+10	0.360	0.000
835.0	4.312E+10	0.361	0.980
835.5	6.288E+10	0.352	0.984
836.0	8.593E+10	0.348	0.986
836.5	7.560E+10	0.353	0.985
837.0	4.445E+10	0.356	0.982
837.5	5.322E+10	0.352	0.985
838.0	7.696E+10	0.350	0.986
838.5	7.365E+10	0.354	0.987
839.0	5.069E+10	0.355	0.986
839.5	4.725E+10	0.356	0.987
840.0	5.434E+10	0.353	0.988
840.5	6.203E+10	0.353	0.987
841.0	6.395E+10	0.353	0.000
841.5	6.443E+10	0.353	0.000
842.0	6.455E+10	0.353	0.000
842.5	6.458E+10	0.353	0.000
843.0	5.819E+10	0.356	0.000
843.5	3.742E+10	0.368	0.000
844.0	2.196E+10	0.375	0.992
844.5	4.895E+10	0.361	0.977
845.0	8.489E+10	0.346	0.989
845.5	4.425E+10	0.353	0.972
846.0	2.819E+10	0.340	0.973
846.5	3.891E+10	0.303	0.974
847.0	8.940E+10	0.285	0.977
847.5	1.752E+11	0.280	0.986
848.0	2.286E+11	0.282	0.984
848.5	2.523E+11	0.280	0.987
849.0	2.239E+11	0.276	0.986
849.5	3.135E+11	0.290	0.986
850.0	4.277E+11	0.293	0.990
850.5	3.879E+11	0.289	0.994
851.0	2.190E+11	0.283	0.986
851.5	2.435E+11	0.292	0.987
852.0	3.443E+11	0.294	0.995
852.5	3.165E+11	0.295	0.996

853.0	2.121E+11	0.295	0.992
853.5	2.078E+11	0.308	0.992
854.0	2.508E+11	0.312	0.994
854.5	2.599E+11	0.325	0.998
855.0	2.269E+11	0.325	0.997
855.5	1.634E+11	0.308	0.995
856.0	1.261E+11	0.285	0.989
856.5	2.021E+11	0.279	0.989
857.0	2.400E+11	0.284	0.992
857.5	1.751E+11	0.285	0.985
858.0	1.480E+11	0.279	0.983
858.5	2.626E+11	0.289	0.995
859.0	4.497E+11	0.293	0.995
859.5	4.541E+11	0.287	0.992
860.0	3.010E+11	0.284	0.994
860.5	2.931E+11	0.304	0.993
861.0	3.721E+11	0.308	0.995
861.5	4.561E+11	0.310	0.997
862.0	4.218E+11	0.313	0.998
862.5	3.609E+11	0.318	0.998
863.0	2.988E+11	0.309	0.997
863.5	3.246E+11	0.315	0.998
864.0	3.306E+11	0.315	0.996
864.5	2.671E+11	0.299	0.995
865.0	1.865E+11	0.287	0.993
865.5	2.232E+11	0.315	0.997
866.0	2.538E+11	0.343	0.997
866.5	2.410E+11	0.327	0.996
867.0	2.203E+11	0.298	0.997
867.5	2.434E+11	0.302	0.998
868.0	2.886E+11	0.302	0.998
868.5	3.260E+11	0.307	0.999
869.0	3.383E+11	0.303	0.999
869.5	2.796E+11	0.307	0.998
870.0	2.352E+11	0.304	0.998
870.5	2.847E+11	0.312	0.998
871.0	3.287E+11	0.313	0.999
871.5	2.642E+11	0.310	0.998
872.0	1.629E+11	0.303	0.997
872.5	1.892E+11	0.317	0.997
873.0	2.561E+11	0.323	0.998
873.5	2.375E+11	0.318	0.998
874.0	1.640E+11	0.310	0.997
874.5	1.875E+11	0.315	0.997
875.0	2.426E+11	0.312	0.998
875.5	2.786E+11	0.320	0.999
876.0	2.670E+11	0.324	0.000
876.5	2.257E+11	0.321	0.998
877.0	1.896E+11	0.319	0.998
877.5	2.408E+11	0.333	0.998
878.0	2.797E+11	0.339	0.999
878.5	2.450E+11	0.336	0.998
879.0	1.643E+11	0.328	0.998
879.5	2.014E+11	0.340	0.998

880.0	2.584E+11	0.349	0.998
880.5	2.312E+11	0.350	0.998
881.0	1.591E+11	0.346	0.998
881.5	1.522E+11	0.359	0.998
882.0	1.749E+11	0.362	0.998
882.5	1.872E+11	0.368	0.998
883.0	1.731E+11	0.368	0.998
883.5	1.563E+11	0.371	0.998
884.0	1.330E+11	0.366	0.997
884.5	1.531E+11	0.375	0.997
885.0	1.793E+11	0.376	0.997
885.5	1.528E+11	0.373	0.997
886.0	9.979E+10	0.366	0.997
886.5	1.181E+11	0.375	0.997
887.0	1.470E+11	0.376	0.998
887.5	1.359E+11	0.368	0.998
888.0	1.017E+11	0.359	0.998
888.5	1.033E+11	0.367	0.998
889.0	1.119E+11	0.365	0.998
889.5	1.109E+11	0.361	0.998
890.0	9.903E+10	0.358	0.997
890.5	8.922E+10	0.361	0.996
891.0	7.683E+10	0.358	0.995
891.5	9.450E+10	0.368	0.995
892.0	1.042E+11	0.372	0.996
892.5	9.125E+10	0.375	0.994
893.0	6.500E+10	0.368	0.995
893.5	7.201E+10	0.382	0.995
894.0	8.057E+10	0.385	0.995
894.5	7.099E+10	0.377	0.995
895.0	5.605E+10	0.366	0.994
895.5	5.962E+10	0.374	0.993
896.0	6.680E+10	0.373	0.995
896.5	6.888E+10	0.375	0.994
897.0	6.361E+10	0.372	0.995
897.5	5.856E+10	0.372	0.995
898.0	4.881E+10	0.370	0.995
898.5	5.507E+10	0.385	0.995
899.0	6.169E+10	0.382	0.995
899.5	6.231E+10	0.367	0.989
900.0	4.633E+10	0.360	0.988
900.5	4.638E+10	0.371	0.989
901.0	4.153E+10	0.367	0.986
901.5	3.511E+10	0.371	0.980
902.0	3.748E+10	0.362	0.000
902.5	4.999E+10	0.329	0.000
903.0	9.493E+10	0.297	0.980
903.5	1.536E+11	0.283	0.993
904.0	1.426E+11	0.281	0.990
904.5	1.533E+11	0.283	0.993
905.0	1.514E+11	0.278	0.990
905.5	2.128E+11	0.285	0.996
906.0	2.275E+11	0.286	0.995
906.5	1.774E+11	0.278	0.994

907.0	1.150E+11	0.275	0.990
907.5	1.721E+11	0.279	0.995
908.0	2.451E+11	0.277	0.995
908.5	2.250E+11	0.274	0.994
909.0	1.554E+11	0.273	0.993
909.5	2.028E+11	0.284	0.996
910.0	2.662E+11	0.289	0.995
910.5	2.711E+11	0.291	0.997
911.0	1.778E+11	0.282	0.996
911.5	1.310E+11	0.285	0.000
912.0	1.347E+11	0.289	0.991
912.5	2.010E+11	0.289	0.997
913.0	2.179E+11	0.291	0.996
913.5	1.858E+11	0.290	0.995
914.0	1.480E+11	0.286	0.993
914.5	1.985E+11	0.297	0.995
915.0	2.472E+11	0.299	0.997
915.5	2.058E+11	0.299	0.996
916.0	1.297E+11	0.299	0.993
916.5	1.578E+11	0.310	0.995
917.0	2.120E+11	0.309	0.997
917.5	2.114E+11	0.312	0.997
918.0	1.686E+11	0.311	0.997
918.5	1.494E+11	0.318	0.997
919.0	1.421E+11	0.315	0.997
919.5	1.597E+11	0.324	0.996
920.0	1.652E+11	0.325	0.997
920.5	1.423E+11	0.325	0.997
921.0	1.006E+11	0.321	0.995
921.5	1.349E+11	0.326	0.996
922.0	1.657E+11	0.326	0.997
922.5	1.541E+11	0.324	0.997
923.0	1.136E+11	0.322	0.996
923.5	8.513E+10	0.335	0.996
924.0	8.946E+10	0.325	0.994
924.5	9.995E+10	0.315	0.993
925.0	7.792E+10	0.312	0.991
925.5	6.747E+10	0.314	0.992
926.0	6.386E+10	0.307	0.989
926.5	5.680E+10	0.305	0.983
927.0	8.373E+10	0.294	0.983
927.5	8.484E+10	0.292	0.984
928.0	5.895E+10	0.292	0.978
928.5	8.320E+10	0.296	0.984
929.0	9.625E+10	0.295	0.987
929.5	8.335E+10	0.292	0.988
930.0	5.756E+10	0.295	0.983
930.5	7.430E+10	0.304	0.984
931.0	7.827E+10	0.300	0.987
931.5	6.334E+10	0.294	0.984
932.0	7.804E+10	0.284	0.984
932.5	1.010E+11	0.284	0.987
933.0	1.207E+11	0.278	0.988
933.5	1.751E+11	0.280	0.988

934.0	2.160E+11	0.279	0.988
934.5	1.904E+11	0.277	0.991
935.0	1.328E+11	0.279	0.989
935.5	1.953E+11	0.285	0.992
936.0	2.321E+11	0.279	0.994
936.5	1.722E+11	0.269	0.000
937.0	1.317E+11	0.266	0.991
937.5	1.931E+11	0.271	0.992
938.0	2.714E+11	0.269	0.994
938.5	2.572E+11	0.271	0.995
939.0	1.914E+11	0.272	0.992
939.5	1.946E+11	0.277	0.993
940.0	2.084E+11	0.275	0.992
940.5	2.562E+11	0.281	0.996
941.0	2.096E+11	0.284	0.996
941.5	1.494E+11	0.288	0.992
942.0	1.321E+11	0.277	0.000
942.5	1.287E+11	0.267	0.981
943.0	1.346E+11	0.262	0.982
943.5	1.160E+11	0.255	0.981
944.0	6.863E+10	0.251	0.979
944.5	6.991E+10	0.255	0.000
945.0	8.326E+10	0.258	0.972
945.5	8.564E+10	0.255	0.975
946.0	7.939E+10	0.257	0.969
946.5	1.016E+11	0.265	0.978
947.0	1.371E+11	0.259	0.973
947.5	2.067E+11	0.255	0.980
948.0	2.019E+11	0.251	0.986
948.5	1.408E+11	0.254	0.986
949.0	1.038E+11	0.256	0.981
949.5	1.619E+11	0.260	0.984
950.0	2.165E+11	0.255	0.985
950.5	1.967E+11	0.250	0.986
951.0	1.414E+11	0.252	0.975
951.5	2.332E+11	0.254	0.983
952.0	3.088E+11	0.252	0.988
952.5	2.907E+11	0.251	0.994
953.0	2.077E+11	0.256	0.982
953.5	2.210E+11	0.264	0.988
954.0	2.419E+11	0.263	0.989
954.5	2.809E+11	0.265	0.995
955.0	2.522E+11	0.264	0.994
955.5	1.950E+11	0.264	0.991
956.0	1.531E+11	0.260	0.992
956.5	1.882E+11	0.265	0.991
957.0	2.052E+11	0.266	0.989
957.5	1.819E+11	0.261	0.990
958.0	1.306E+11	0.256	0.992
958.5	1.489E+11	0.270	0.993
959.0	1.606E+11	0.272	0.991
959.5	1.454E+11	0.266	0.994
960.0	1.157E+11	0.266	0.989
960.5	1.183E+11	0.272	0.987

961.0	1.159E+11	0.270	0.986
961.5	1.028E+11	0.269	0.981
962.0	9.640E+10	0.269	0.981
962.5	8.380E+10	0.272	0.979
963.0	6.898E+10	0.268	0.978
963.5	9.895E+10	0.263	0.984
964.0	1.173E+11	0.262	0.982
964.5	1.141E+11	0.261	0.985
965.0	7.748E+10	0.262	0.981
965.5	1.039E+11	0.265	0.984
966.0	1.187E+11	0.262	0.983
966.5	1.036E+11	0.259	0.983
967.0	8.938E+10	0.260	0.981
967.5	9.858E+10	0.266	0.983
968.0	7.662E+10	0.265	0.979
968.5	5.443E+10	0.261	0.972
969.0	6.412E+10	0.259	0.966
969.5	6.781E+10	0.264	0.969
970.0	6.587E+10	0.260	0.971
970.5	1.343E+11	0.253	0.977
971.0	2.153E+11	0.250	0.978
971.5	2.031E+11	0.248	0.988
972.0	1.550E+11	0.255	0.976
972.5	2.956E+11	0.257	0.989
973.0	3.893E+11	0.253	0.994
973.5	3.132E+11	0.251	0.994
974.0	2.251E+11	0.252	0.986
974.5	2.589E+11	0.257	0.992
975.0	3.099E+11	0.261	0.997
975.5	3.476E+11	0.271	0.999
976.0	3.153E+11	0.277	0.999
976.5	2.868E+11	0.277	0.999
977.0	2.561E+11	0.268	0.997
977.5	3.336E+11	0.276	0.999
978.0	3.405E+11	0.288	0.999
978.5	2.859E+11	0.283	0.998
979.0	1.938E+11	0.277	0.997
979.5	2.536E+11	0.295	0.998
980.0	2.811E+11	0.303	0.999
980.5	2.165E+11	0.300	0.995
981.0	1.748E+11	0.287	0.998
981.5	2.054E+11	0.287	0.996
982.0	2.381E+11	0.285	0.998
982.5	2.457E+11	0.290	0.998
983.0	2.347E+11	0.289	0.000
983.5	1.933E+11	0.281	0.000
984.0	1.814E+11	0.282	0.998
984.5	2.330E+11	0.299	0.998
985.0	2.530E+11	0.306	0.998
985.5	2.149E+11	0.297	0.998
986.0	1.641E+11	0.289	0.998
986.5	2.157E+11	0.308	0.997
987.0	2.440E+11	0.310	0.998
987.5	2.024E+11	0.300	0.998

988.0	1.561E+11	0.295	0.997
988.5	1.630E+11	0.310	0.997
989.0	1.837E+11	0.293	0.997
989.5	1.977E+11	0.269	0.997
990.0	2.032E+11	0.273	0.997
990.5	1.725E+11	0.286	0.996
991.0	1.418E+11	0.271	0.991
991.5	1.915E+11	0.261	0.996
992.0	1.992E+11	0.256	0.994
992.5	1.312E+11	0.250	0.993
993.0	1.134E+11	0.251	0.984
993.5	1.863E+11	0.260	0.992
994.0	2.281E+11	0.255	0.992
994.5	2.004E+11	0.246	0.998
995.0	1.707E+11	0.253	0.985
995.5	2.219E+11	0.259	0.997
996.0	2.099E+11	0.253	0.995
996.5	2.015E+11	0.253	0.992
997.0	2.238E+11	0.252	0.994
997.5	2.398E+11	0.250	0.997
998.0	2.104E+11	0.249	0.998
998.5	2.448E+11	0.260	0.995
999.0	2.587E+11	0.260	0.998
999.5	2.132E+11	0.259	0.997
1000.0	1.666E+11	0.255	0.998
1000.5	1.998E+11	0.273	0.995
1001.0	1.987E+11	0.272	0.995
1001.5	1.526E+11	0.260	0.995
1002.0	1.279E+11	0.257	0.991
1002.5	1.615E+11	0.262	0.991
1003.0	2.114E+11	0.258	0.993
1003.5	2.170E+11	0.252	0.993
1004.0	2.275E+11	0.252	0.995
1004.5	2.445E+11	0.257	0.994
1005.0	2.403E+11	0.254	0.993
1005.5	2.890E+11	0.256	0.998
1006.0	2.621E+11	0.262	0.995
1006.5	2.118E+11	0.265	0.996
1007.0	1.688E+11	0.264	0.994
1007.5	2.197E+11	0.268	0.996
1008.0	2.386E+11	0.263	0.998
1008.5	1.886E+11	0.261	0.997
1009.0	1.468E+11	0.267	0.992
1009.5	1.618E+11	0.282	0.997
1010.0	1.674E+11	0.281	0.998
1010.5	1.429E+11	0.277	0.997
1011.0	1.315E+11	0.280	0.998
1011.5	1.283E+11	0.285	0.996
1012.0	1.307E+11	0.279	0.998
1012.5	1.344E+11	0.283	0.998
1013.0	1.295E+11	0.288	0.998
1013.5	1.144E+11	0.289	0.996
1014.0	8.723E+10	0.285	0.997
1014.5	9.811E+10	0.290	0.995

1015.0	1.184E+11	0.282	0.995
1015.5	1.028E+11	0.274	0.997
1016.0	8.905E+10	0.274	0.995
1016.5	1.110E+11	0.280	0.993
1017.0	1.215E+11	0.276	0.994
1017.5	1.077E+11	0.275	0.994
1018.0	9.631E+10	0.273	0.996
1018.5	8.831E+10	0.270	0.997
1019.0	8.175E+10	0.269	0.997
1019.5	8.963E+10	0.278	0.998
1020.0	9.029E+10	0.285	0.997
1020.5	8.385E+10	0.281	0.997
1021.0	7.213E+10	0.274	0.998
1021.5	7.057E+10	0.290	0.996
1022.0	6.392E+10	0.295	0.994
1022.5	5.386E+10	0.285	0.997
1023.0	4.418E+10	0.289	0.992
1023.5	5.393E+10	0.286	0.993
1024.0	5.534E+10	0.282	0.996
1024.5	4.461E+10	0.289	0.994
1025.0	4.392E+10	0.292	0.995
1025.5	4.134E+10	0.298	0.996
1026.0	3.183E+10	0.303	0.996
1026.5	3.395E+10	0.303	0.000
1027.0	3.713E+10	0.300	0.996
1027.5	3.294E+10	0.293	0.996
1028.0	2.683E+10	0.286	0.985
1028.5	2.966E+10	0.280	0.984
1029.0	2.991E+10	0.272	0.972
1029.5	4.158E+10	0.240	0.966
1030.0	5.976E+10	0.224	0.974
1030.5	1.062E+11	0.235	0.980
1031.0	1.394E+11	0.232	0.983
1031.5	1.151E+11	0.231	0.973
1032.0	1.285E+11	0.234	0.974
1032.5	1.422E+11	0.239	0.976
1033.0	1.799E+11	0.230	0.981
1033.5	2.594E+11	0.226	0.992
1034.0	3.098E+11	0.231	0.988
1034.5	2.916E+11	0.232	0.991
1035.0	2.369E+11	0.235	0.985
1035.5	3.428E+11	0.239	0.991
1036.0	3.825E+11	0.237	0.995
1036.5	3.150E+11	0.237	0.993
1037.0	2.862E+11	0.241	0.992
1037.5	3.576E+11	0.262	0.997
1038.0	3.708E+11	0.256	0.999
1038.5	3.110E+11	0.247	0.993
1039.0	3.456E+11	0.250	0.996
1039.5	3.646E+11	0.257	0.997
1040.0	3.741E+11	0.248	0.997
1040.5	3.972E+11	0.250	0.999
1041.0	4.305E+11	0.256	0.997
1041.5	4.091E+11	0.259	0.999

1042.0	3.191E+11	0.260	0.998
1042.5	3.101E+11	0.268	0.997
1043.0	2.281E+11	0.266	0.997
1043.5	8.256E+10	0.238	0.954
1044.0	7.482E+10	0.222	0.961
1044.5	1.559E+11	0.227	0.971
1045.0	2.909E+11	0.216	0.971
1045.5	3.559E+11	0.202	0.997
1046.0	3.621E+11	0.221	0.967
1046.5	5.372E+11	0.228	0.997
1047.0	5.716E+11	0.228	0.985
1047.5	7.089E+11	0.221	0.997
1048.0	7.635E+11	0.226	0.996
1048.5	6.203E+11	0.232	0.995
1049.0	4.254E+11	0.237	0.983
1049.5	4.772E+11	0.244	0.984
1050.0	5.272E+11	0.241	0.997
1050.5	4.660E+11	0.228	0.999
1051.0	3.813E+11	0.236	0.997
1051.5	4.415E+11	0.253	0.999
1052.0	4.083E+11	0.252	0.998
1052.5	3.103E+11	0.244	0.999
1053.0	3.229E+11	0.249	0.992
1053.5	4.120E+11	0.248	0.999
1054.0	3.873E+11	0.243	0.999
1054.5	3.445E+11	0.241	0.995
1055.0	4.204E+11	0.239	0.998
1055.5	3.607E+11	0.245	0.988
1056.0	3.299E+11	0.247	0.988
1056.5	3.981E+11	0.256	0.999
1057.0	3.714E+11	0.259	0.999
1057.5	2.762E+11	0.249	0.993
1058.0	2.862E+11	0.242	0.992
1058.5	4.173E+11	0.247	0.999
1059.0	4.101E+11	0.248	0.998
1059.5	3.166E+11	0.241	0.996
1060.0	3.862E+11	0.249	0.997
1060.5	4.695E+11	0.267	0.999
1061.0	4.718E+11	0.266	0.998
1061.5	4.530E+11	0.266	0.999
1062.0	4.821E+11	0.267	0.999
1062.5	4.259E+11	0.256	0.999
1063.0	3.087E+11	0.255	0.996
1063.5	3.131E+11	0.267	0.997
1064.0	3.410E+11	0.268	0.996
1064.5	3.118E+11	0.257	0.995
1065.0	2.952E+11	0.256	0.997
1065.5	3.308E+11	0.273	0.998
1066.0	3.003E+11	0.270	0.999
1066.5	2.558E+11	0.244	0.998

<b>REPORT DOCUMENTATION PAGE</b>			<i>Form Approved</i> OMB No. 0704-0188	
Public reporting burden for this collection of information is estimated to average 1 hour per response, including the time for reviewing instructions, searching existing data sources, Gathering and maintaining the data needed, and completing and reviewing the collection of information. Send comments regarding this burden estimate or any other aspect of this collection of information, including suggestions for reducing this burden, to Washington Headquarters Services, Directorate for Information Operation and Reports, 1215 Jefferson Davis Highway, Suite 1204, Arlington, VA 22202-4302, and to the Office of Management and Budget, Paperwork Reduction Project (0704-0188), Washington, DC 20503				
<b>1. AGENCY USE ONLY (Leave Blank)</b>	<b>2. REPORT DATE</b> June 2004	<b>3. REPORT TYPE AND DATES COVERED</b> Contractor Report		
<b>4. TITLE AND SUBTITLE</b> Mining CRRES IDM Pulse Data and CRRES Environmental Data to Improve Spacecraft Charging/Discharging Models and Guidelines			<b>5. FUNDING NUMBERS</b>  H-34774D	
<b>6. AUTHORS</b> A.R. Frederickson and D.H. Brautigam*				
<b>7. PERFORMING ORGANIZATION NAMES(S) AND ADDRESS(ES)</b> Caltech Jet Propulsion Laboratory *Space Vehicles Directorate California Institute of Technology USAF Research Laboratories Pasadena, CA 91109-8099 Hanscom Air force Base, MA 01731			<b>8. PERFORMING ORGANIZATION REPORT NUMBER</b>  M-1111	
<b>9. SPONSORING/MONITORING AGENCY NAME(S) AND ADDRESS(ES)</b> NASA's Space Environments and Effects (SEE) Program George C. Marshall Space Flight Center Marshall Space Flight Center, AL 35812			<b>10. SPONSORING/MONITORING AGENCY REPORT NUMBER</b>  NASA/CR-2004-213228	
<b>11. SUPPLEMENTARY NOTES</b> Prepared for NASA's Space Environments and Effects (SEE) Program by Caltech Jet Propulsion Laboratory Technical Monitor: Donna Hardage, NASA Marshall Space Flight Center				
<b>12a. DISTRIBUTION/AVAILABILITY STATEMENT</b> Unclassified-Unlimited Subject Category 93 Availability: NASA CASI (301) 621-0390			<b>12b. DISTRIBUTION CODE</b>	
<b>13. ABSTRACT (Maximum 200 words)</b>  One can truly predict the charging and pulsing in space over a year's time using only the physics that worked for periods of an hour and less in prior publications. All portions of the task were achieved, including the optional portion of determining a value for conductivity that best fit the data.  Fortran statements were developed that are required for the NUMIT runs to work with this kind of data from space. In addition to developing the Fortran for NUMIT, simple correlations between the IDM pulsing history and the space radiation were observed because we now have a better characterization of the space radiation.  The study showed that: (1) the new methods for measurement of charge storage and conduction in insulators provide the correct values to use for prediction of charging and pulsing in space; (2) the methods in NUMIT that worked well for time durations less than hours now work well for durations of months; (3) an average spectrum such as AE8 is probably not a good guide for predicting pulsing in space—one must take time dependence into account in order to understand insulator pulsing; and (4) the old method for predicting pulse rates in space that was based on the CRRES data could be improved to include dependencies on material parameters.				
<b>14. SUBJECT TERMS</b> pulse data, charging, discharging, high energy, electrons, electric field, internal discharge monitor, CRRES			<b>15. NUMBER OF PAGES</b> 53	
			<b>16. PRICE CODE</b>	
<b>17. SECURITY CLASSIFICATION OF REPORT</b> Unclassified	<b>18. SECURITY CLASSIFICATION OF THIS PAGE</b> Unclassified	<b>19. SECURITY CLASSIFICATION OF ABSTRACT</b> Unclassified	<b>20. LIMITATION OF ABSTRACT</b> Unlimited	